Investigation of island/ single core and archipelago/ multicore enriched asphaltenes and their solubility fractions by thermal analysis coupled to high resolution Fourier transform ion cyclotron resonance mass spectrometry

Anika Neumann[1,2], Martha Liliana Chacón-Patiño[3], Ryan P. Rodgers[3], Christopher P. Rüger[1,2]*, Ralf Zimmermann[1,2,4]

1 –Joint Mass Spectrometry Centre (JMSC)/Chair of Analytical Chemistry, University of Rostock, 18059 Rostock, Germany

2 – Department Life, Light & Matter (LLM), University of Rostock, 18051 Rostock, Germany

3 – National High Magnetic Field Laboratory and Florida State University, Tallahassee, Florida 32310, United States

4 – Joint Mass Spectrometry Centre (JMSC)/Helmholtz Zentrum München, Comprehensive Molecular Analytics, 85764 Neuherberg, Germany

Keywords: asphaltenes, thermal analysis, high-resolution mass spectrometry, pyrolysis, extrography

* corresponding author, christopher.rueger@uni-rostock.de

Abstract

Despite extensive research, the molecular-level chemical characterization of asphaltenes, a highly aromatic solubility fraction of petroleum, remains an analytical challenge. This fraction is related to diverse problems in crude oil exploration, transportation, and refining. Two asphaltene architecture motifs are commonly discussed in literature, “island” (single core) and “archipelago” (multicore) type structures. The thermal desorption and pyrolysis behavior of island- and archipelago-enriched asphaltenes and their extrography fractions was investigated. For this purpose, the evolved chemical pattern was investigated by thermal analysis coupled to ultrahigh resolution mass spectrometry (FT-ICR MS). Soft atmospheric pressure chemical ionization preserved the molecular information of the thermal emission profile. Time/temperature-resolved analysis allowed the chemical characterization of occluded material as well as of asphaltene building blocks during pyrolysis.

Regarding the thermogravimetric information, the island-type enriched sample (Wyoming asphaltenes) revealed a significantly higher coke residue after the pyrolysis process compared to the archipelago-type enriched sample (Athabasca asphaltenes). In contrast to whole asphaltenes, extrographic fractions revealed occluded material evolved during the desorption phase. For the acetone fraction, this effect was most abundant and suggests cooperative aggregation.

Pyrolysis revealed a bimodal behavior for most of the compound classes suggesting the presence of both architecture motifs in each asphaltene. DBE versus #C diagrams of the pyrolysis molecular profile revealed specific compositional trends: compounds with high DBE values and short alkylation likely to be originated from island-type asphaltenes, whereas species with low DBE values and high carbon numbers likely derive from archipelago-type asphaltenes.

In the asphaltene structural debate, thermal analysis ultrahigh resolution mass spectrometry serves as additional technique and supplements results obtainable by other techniques, such as direct infusion approaches. Consistent results on the structural motifs are indicated by the molecular fingerprint visualized by DBE versus #C diagrams and serve as measure for the dominance of a structural motif.

Introduction

During the production, transportation, and refining of crude oils, asphaltenes are often related to problems such as deposit formation, fouling of catalysts, or destabilization of the crude oil mixture. [1–6] Due to the high economic relevance, asphaltenes are therefore of significant interest in petroleum chemistry. However, because of their high chemical and structural complexity, and despite recent advances in mass spectrometry and atomic force microscopy [7–9], asphaltenes remain an analytical challenge.

Asphaltenes are defined as the fraction of crude oil that is soluble in toluene, but insoluble in paraffinic solvents such as n-pentane (C5), cyclo-/n-hexane (C6), and n-heptane (C7). They are composed of peri-condensed aromatic cores with peripheral alkyl chains (island /single-core structural motif) as well as smaller aromatic cores linked by alkyl or naphthenic bridges (archipelago /multicore structural motif) and contain higher amounts of heteroatoms (sulfur, nitrogen, oxygen) and metals (e.g. vanadium and nickel). [10–12] Due to their high aggregation tendency [13,14], the molecular weight range of monomeric asphaltenes was debated for decades. Meanwhile, researchers mostly agree on a mass range of 200-1500 Da with an average molecular weight of 500-800 Da. [15–19]

Not only the asphaltenes' molecular weight was a controversial issue in literature, but also the molecular architecture is still subject of investigation. The island model was introduced in the early 1960s by Yen et al. (1961) [20] and was later modified by Mullins and co-workers [21]. Since then, the island structural motif was supported by a variety of analytical techniques. For example, atomic force microscopy (AFM) predominantly revealed highly per- and cata-condensed PAHs structures with 4-20 fused rings in one aromatic core [7,8]. Nonetheless, AFM is known to be biased towards the detection of planar molecules [22,23], which leads to a favored detection of island structural motifs. Nuclear magnetic resonance (NMR), however, provides additional evidence for single aromatic cores with 4-7 fused rings [11,24,25]. Further, different mass spectrometric techniques with several ionization methods preferentially exhibited island-type asphaltenes. Laser desorption laser ionization mass spectrometry (L^2MS)

of asphaltene model compounds revealed significant similarity of island-type species to the fragmentation behavior of real asphaltene samples [26,27]. Similar results were observed for model compounds as well as asphaltenes by using mass spectrometry with collision-induced dissociation (CID) fragmentation, which results in an average number of 3-8 fused rings with up to 20 carbon atoms in alkyl-side chains. [19,28–30]

Nonetheless, although the island model serves to describe some asphaltene properties, such as reservoir geodynamics, it is incongruent with asphaltene behavior in several scenarios, *e.g.,* products observed after thermal upgrading or pyrolytic degradation. After thermal cracking, the newly formed maltene fraction has been found to consist of alkylated 1-5-ring aromatics, alkanes, and alkenes, as well as naphthenes. [31–36] These observations are supported by Savage et al. (1985/1988), who investigated structural building blocks of pyrolyzed asphaltenes with gas chromatography (GC)-MS [37,38]. Furthermore, Strausz and co-workers provided detailed compositional and structural information on asphaltene pyrolysis products by applying gas chromatographic (GC and GC-MS) as well as spectroscopic techniques. [12,35,39,40] Karimi et al. (2011) found by thin-film pyrolysis small quantitative differences in building blocks revealed from asphaltenes of different geological origin. Rueda-Velásquez et al. (2013) investigated asphaltene building blocks after thermal cracking under hydrogenation conditions. They found small aromatic, alkylated fragments providing evidence for archipelago-type structures, while 35-45 % of the samples remained as high boiling point, highly aromatic compounds. [31]

In the last two decades, high resolution Fourier transformation ion cyclotron resonance mass spectrometry (FT-ICR MS) contributed valuable insights on the asphaltene compositional space due to its ultra-high resolving power and mass accuracy. McKenna et al. (2013) defined the asphaltene compositional space by direct infusion (DI) atmospheric pressure photo ionization (APPI) FT-ICR MS. The authors concluded that asphaltenes are preferentially composed of highly aromatic /alkyl-depleted compounds with double bond equivalents (DBE = number of rings and double bonds to carbon [41]) of over 20 and abundance-weighted H/C ratios between 0.8 to 0.9. [42] Based on these results, it was concluded that

asphaltenes are an extension of the maltene compositional space in aromaticity, but share similar carbon number. [42] Subsequently, Podgorski et al. (2013) revealed, by infrared multiphoton dissociation (IRMPD), evidence for the existence of both structural motifs, due to the presence of fragment ions with prevalent DBE values below 15 (archipelago fragments) as well as highly aromatic compounds with DBEs of up to 25 (island fragments). [43] Further evidence for the presence of archipelago-type asphaltenes were revealed by analyzing the evolved gas mixture of asphaltenes by thermogravimetry (TG) coupled to FT-ICR MS [33,44]. The authors inferred an average archipelago structure composed of three aromatic cores linked by alkyl bridges for the interlaboratory sample known as PetroPhase-2017 asphaltenes [44,45]. McKenna et al. (2019) further concluded the presence of archipelago structures in asphaltenes by observing small thermal fragments during distillation of high petroleum boiling cuts [10]. Recently, the predominance of island-type asphaltenes in DI-FT-ICR MS spectra was found to be caused by efficient ionization, or high monomer ion yield, whereas archipelago-type asphaltenes were revealed to poorly ionize due to a higher aggregation tendency [46,47]. Extrography fractionation of asphaltenes revealed that island and archipelago structural motifs are enriched in different solubility fractions, such as acetone (enriched in species with high monomer ion yield, island dominant) or tetrahydrofuran/methanol (enriched in species with low monomer ion yield, archipelago dominant). [48,49] The predominance of both structures not only depends on the regarded fraction but also on the origin of the asphaltenes as well as the investigated molecular mass range. [50] In a recent study, Athabasca bitumen and Wyoming deposit asphaltenes were investigated by APPI-IRMPD-FT-ICR MS. While Athabasca asphaltenes revealed dominant island- and archipelago-like fragmentation throughout the mass range, Wyoming asphaltenes revealed dominant island-like fragmentation for smaller molecular weight asphaltenes, whereas higher m/z-values exhibited both structural fragmentation pathways. [50]

In this study, we combine the extrography fractionation of asphaltenes from different geological origins [48,50] with temperature resolved analysis by TG-FT-ICR MS to investigate asphaltene solubility fractions enriched in archipelago and island structural motifs. As ionization technique, atmospheric pressure chemical ionization (APCI) was applied, which covers semi-polar to polar compounds expected to be

present in the solubility fractions. It's value for analyzing complex mixtures in combination with TG-FT-ICR MS has been demonstrated in previous studies [33,44,51]. Here, we showed that TG-FT-ICR MS can address the controversial issue of the predominant structural motif of asphaltenes exhibiting corresponding results to previous studies on the same asphaltenes with DI-IRMPD-FT-ICR MS [48,50]. Both investigated asphaltenes obtained from Athabasca bitumen and Wyoming deposit, respectively, revealed differences in the compositional space, the presence of occluded material, and coke formation during evolved gas analysis. Nonetheless, both asphaltenes revealed island- and archipelago-related pyrolysis fragments, whose abundance were found to vary between the geological origin as well as the different solubility fractions.

Material and Methods

Asphaltene Precipitation from Crude Oils.

Asphaltenes were isolated from Athabasca Bitumen and Wyoming petroleum deposit following a slightly adapted version of the standard method D6560-12. [45,52] Briefly, petroleum samples were mixed with n-heptane in a 1/40 volume ratio under sonication and refluxed heating at 85 °C for 1 h. The mixture oil/n-heptane was allowed to settle overnight, protected from light, and subsequently filtrated (Whatman 2 paper filter) to recover the precipitated solids. Asphaltene cleaning was performed in a Soxhlet apparatus with hot n-heptane under nitrogen atmosphere for 120 h. The cleaned C7 insolubles were recovered by dissolution in hot toluene and dried under nitrogen. Solid asphaltenes were subjected to an additional cleaning step, which consists of four cycles of asphaltene crushing and Soxhlet extraction with n-heptane to remove co-precipitated C7 solubles.

Extrography Fractionation.

Extrography is a separation method that involves sample adsorption on a polar adsorbent (e.g., SiO_2, alumina, cellulose), and subsequent desorption with specific solvents. In short, asphaltenes were adsorbed on silica gel with a mass loading of 1 wt. % (10 mg of asphaltenes / 1 g of dried SiO_2); the mixture was dried under nitrogen and then extracted with acetone, n-heptane/toluene (Hep/Tol 1:1 v/v), and toluene/tetrahydrofuran/methanol (Tol/THF/MeOH 10:10:1). The fractions were dried under nitrogen and stored in amber-glass vials. It is essential to point out that using a low mass loading (≤1 wt. %) and drying the silica gel after acetone extraction are essential conditions to optimize the separation process as shown in the literature. [48]

Thermal gravimetry coupled to atmospheric pressure chemical ionization Fourier transform ion cyclotron resonance mass spectrometry (TG-APCI-FT-ICR MS).

Asphaltene samples were investigated by thermal gravimetry (TG) coupled to APCI-FT-ICR MS. A detailed description of the set-up can be found elsewhere [53]. For the asphaltenes, approximately 0.3 to 0.5 mg of the sample material was introduced in an aluminum crucible to the thermo balance (TG 209 cell thermo balance, Netzsch, Selb, Germany) without further sample pre-treatment. The samples were then heated under nitrogen atmosphere with the following temperature program: Starting at 20 °C (held for 2 min), heating from 20 °C to 600 °C with a heating rate of 5 K/min (held for 10 min). The evolved gas mixture was transferred to the ionization chamber of the mass spectrometer via a slight overpressure over a heated transfer line (8 mbar, 300 °C). Positive mode APCI was carried out using a modified GC-APCI II ion source (Bruker Daltonics, Bremen, Germany) with a corona needle current of 3000 µa. The sample was transported by a high nebulizer gas stream of 5 l/min to suppress contamination signals of the ion source. Dry gas flow was set to 3 l/min. The performance of the instrumentation was checked each day by measuring polystyrene (Sigma Aldrich) as standard. [33,44]

Temperature-resolved mass spectra were recorded using a 7 Tesla Fourier transform ion cyclotron resonance mass spectrometry (APEX Qe, Bruker Daltonics, Bremen, Germany). Spectra were acquired with a 2-second transient (4 Megaword) resulting in a mass resolution of 260,000 @*m/z* 400. To enhance the signal-to-noise ratio, 10 microscans were acquired resulting in one mass spectrum every 20 seconds. Data processing was carried out using Bruker DataAnalysis 5.1 for pre-calibration of the average mass spectra and subsequent export of the line spectra. Data were further processed with the self-written program CERES, which is based on MATLAB scripting (MATLAB 2019b). Blank correction was carried out on mass list level before sum formula calculation to avoid misassignments of contaminants. Each single spectrum was individually recalibrated on internal homologues series and normalized on the weight portion of the sample. Time-resolved features were then traced with a feature error border of 5 ppm and a sum formula error of 1 ppm. Sum formulae were assigned using the following restrictions: #C 4-100, #H 4-200, #N 0-1, #O 0-2, #S 0-3, H/C ratio 0.4-2.4, ring and double bond equivalent (DBE) 0-40, and *m/z* range 100-1000.

Results and discussion

Athabasca asphaltenes, a sample highly enriched in archipelago-type compounds, and Wyoming asphaltenes, highly enriched in island-type structural motifs, were fractionated by extrography [50]. In the present study, the whole asphaltenes were compared to their solubility fractions distinctly differing in compositional space [50], which are, in particular, the acetone-soluble fraction, the heptane/toluene-soluble (Hep/Tol) fraction, and the tetrahydrofuran/toluene/methanol-soluble (THF/Tol/MeOH) fraction. Table 1 presents the total recovery of the fractionation procedure, as well as the weight-% of the investigated fractions. Wyoming asphaltenes were enriched in the acetone fraction with 35.4 wt.-%, while Athabasca asphaltenes revealed 24.1 wt.-%. The latter value is in accordance with Peng et al. (1997), who revealed that 20 wt.-% of Athabasca asphaltenes was extractable with acetone [54]. The

Hep/Tol-fraction comprised 23.2 wt.-% for Athabasca and 36 wt.-% for Wyoming asphaltenes, respectively. Athabasca asphaltenes are enriched in compounds extracted by Tol/THF/MeOH (43.5 wt.-%) compared to 25.1 wt.-% for the Wyoming asphaltenes.

Table 1: Overview on the total recovery and weight-% of the fractions obtained by extrography fractionation as well as percentage of mass loss and the maximum mass loss temperature revealed by thermal gravimetry.

	Athabasca			
	whole sample	Acetone	Hep/Tol	THF/Tol/MeOH
total recovery [%]/ weight-% fraction*	90.8	24.1	23.2	43.5
max. mass loss temp. [°C]	430	420	430	420
mass loss [%]	50	61	62	63
	Wyoming			
total recovery [%]/ weight-% fraction*	96.5	35.4	36.0	25.1
max. mass loss temp. [°C]	435	450	450	440
mass loss [%]	22	43	36	41

*values taken from Chacón-Patiño et al. [50]

The pyrolysis of asphaltenes was applied for decades to investigate their structural building blocks and to reduce their chemical complexity hardly accessible comprehensively by any analytical technique [11,32,36,37,39,55]. Figure 1 depicts the three main pathways asphaltenes undergo during evolved gas analysis: (1) Low-molecular weight compounds, typically present in the maltene fraction, were shown to evaporate intact [33]. With regard to the investigated asphaltenes, primarily occluded maltenes release should occur in the desorption phase [33]. The structures presented in Figure 1 are based on exemplary sum formula assignments and DBE values of asphaltene compounds investigated in this study as well as structural moieties described in the literature for crude oils and asphaltenes [12,35,39,54,56,57]. (2) From 300 to 350 °C, pyrolysis of asphaltenes starts by thermal decomposition of C-C- and C-S-bonds [58], releasing smaller structural elements in the gas phase. Archipelago-type structures are preferably cracked at alkyl linkers between two smaller core structures [10,34]. Island-type structural motifs, however, are known to cleave off alkyl side chains during thermal treatment [34,59–61] resulting in lowly alkylated, highly aromatic cores clustering at the aromatic limit [62–64] as well as aliphatic compounds. If the aromatic core of island-type asphaltenes is still evaporable, it is detected during the pyrolysis phase, otherwise, (3) extremely highly aromatic cores (high boiling point)

tend to form coke and remain as residue [34,59,60]. Furthermore, highly stable aggregates may survive high temperatures during the pyrolysis phase and form coke instead of thermally decompose into smaller fragments [65].

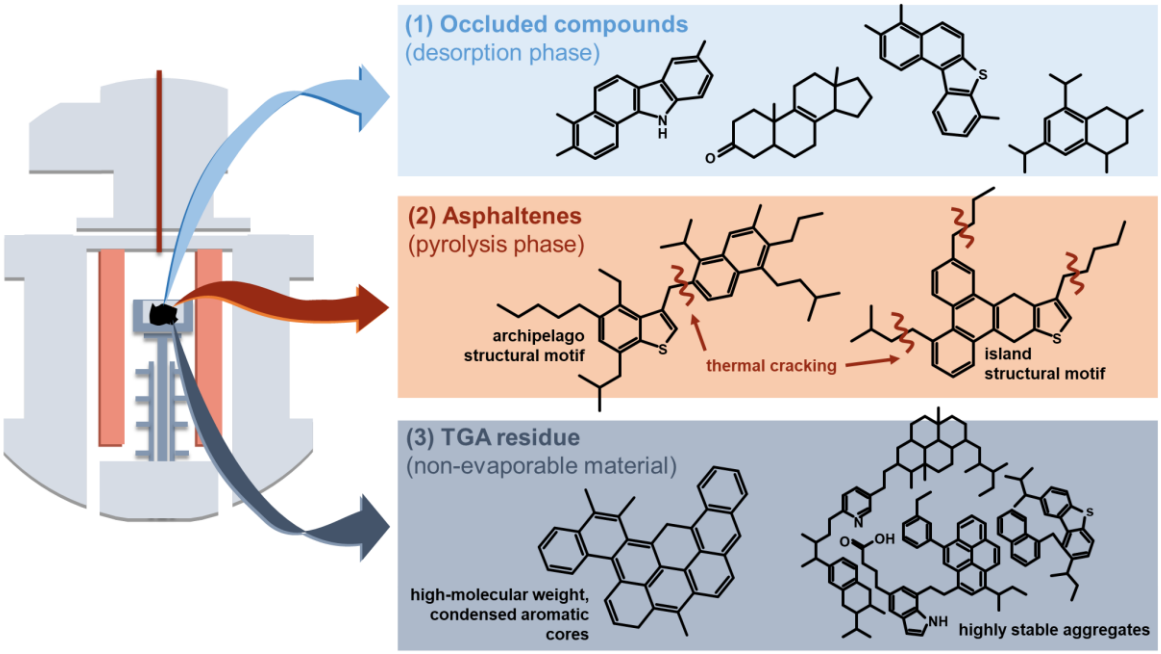

Figure 1: Schematic representation of the primary evolved gas analysis pathways. (1) Low molecular weight compounds are evaporated intact in the desorption phase. (2) During the pyrolysis phase, asphaltenes are cracked releasing smaller building blocks. (3) Extremely high aromatic compounds tend to form coke, which remains as TGA residue.

Thermal gravimetric analysis (TGA) was frequently used for asphaltenes to determine mass loss, coke yield, and the maximum mass loss temperature in the literature [33,44,55,66]. By applying a thermobalance, mass loss can be traced with increasing temperature in real-time resulting in a mass loss diagram; whereas the differential thermogravimetric (DTG) signal reveals the mass loss rate. Figure 2 shows the mass loss and DTG diagrams of the studied Athabasca and Wyoming asphaltenes and their fractions. Both unfractionated asphaltenes reveal a considerable mass loss between 300-500 °C. Friesen et al. (2005) already reported for Athabasca asphaltenes that all pyrolyzable material is decomposed below 525 °C [67], while Huang et al. (2007) found that thermal decomposition occurred primarily between 350-450 °C for Florida asphaltenes [68].

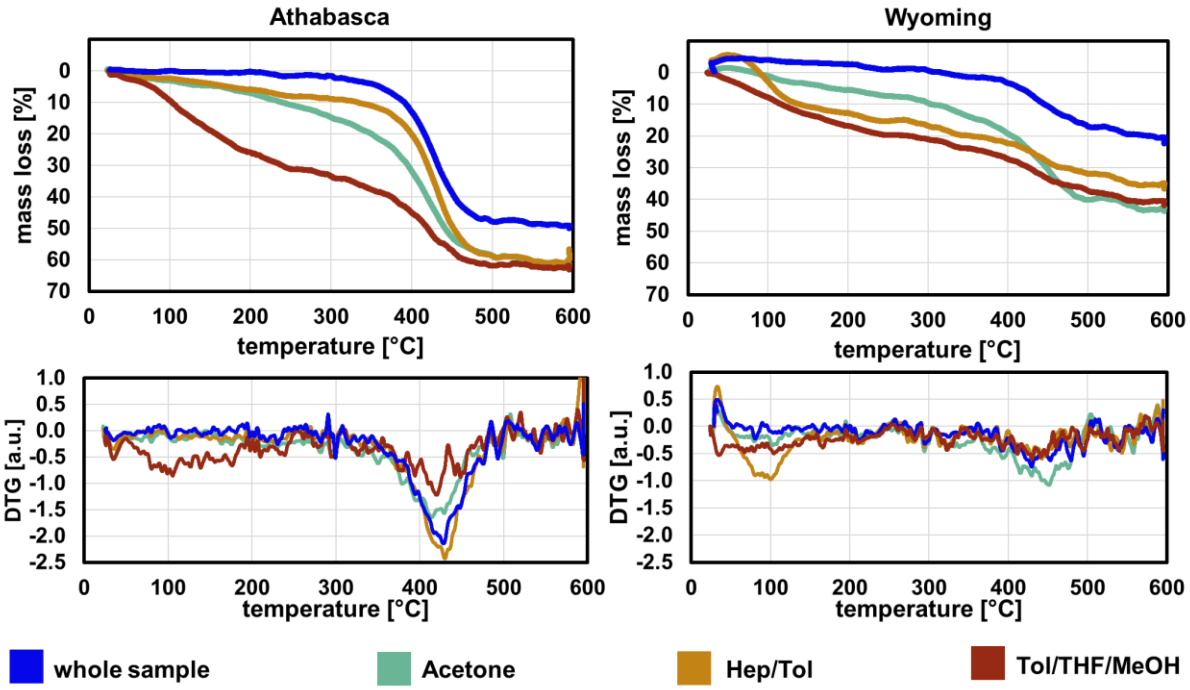

Figure 2: Mass loss diagrams and corresponding DTG signals during TGA of Athabasca and Wyoming asphaltenes and their respective extrography fractions.

In contrast to the whole asphaltenes, the polarity fractions revealed a mass loss below 300 °C indicating the release of enriched occluded material later discussed in detail. This result is consistent with the supramolecular assembly model for aggregation of asphaltenes introduced by Gray et al. (2011) [65]. The model implies the occlusion of maltene compounds by *e.g.* acid-base interactions, hydrogen bonding, or metal coordination, in addition to the well-known π-π-stacking [65,69]. We hypothesize that during extrography, aggregates are dispersed allowing the release of smaller occluded material at lower temperatures. Strikingly, Athabasca asphaltenes revealed for all samples substantially higher mass losses of 50-63 % than Wyoming asphaltenes with 22-43 %. The difference implies that Wyoming asphaltenes are enriched in components that form non-distillable residues during thermal treatment, such as coke precursors, non-evaporable organic species, compounds with slow pyrolysis rates, or inorganic material. [33,70,71] It is known that asphaltenes from different geological origins yield in different amounts of coke/TGA residue [31–33,72], but also various pyrolysis conditions result in the wide range of residue yields of 35-75 % reported in the literature [36]. The TGA residues for Athabasca asphaltenes

(47-50 %) and Wyoming asphaltenes (57-78 %) obtained in this study are consistent with values revealed in earlier studies. Rueda-Velàsques et al. (2013) and Karimi et al. (2011) reported 46-47 % coke yield for Athabasca asphaltenes [31,32], whereas Juyal et al. (2013) reported 69 % for Wyoming asphaltenes [71]. Concerning the DTG diagrams, Athabasca asphaltenes showed a lower temperature for the maximum weight loss from 420-430 °C than Wyoming asphaltenes from 435-450 °C. Slightly higher values for the maximum weight loss temperature are found in earlier studies on other asphaltenes, such as Maya asphaltenes (478 °C) [55], Cold Lake bitumen asphaltenes (480 °C) [55] as well as asphaltenes from Garzan (468 °C) and Raman (458 °C) crude oils [66]. Although Maya and Cold Lake bitumen asphaltenes are known for high concentration of archipelago structural motifs, the reported maximum weight loss temperatures are slightly higher. However, besides the different geological origin of the asphaltenes, the heating rate of the TGA is different compared to the present study (10 K/min versus 5 K/min), which could explain the observed variations. Regarding the different extrographic fractions investigated in this study, both asphaltenes exhibited a higher TGA residue for the whole sample. Without fractionation, Athabasca asphaltenes yield 50 % residue, while all fractions revealed approximately 40 % residue formation. Similar results can be observed for Wyoming asphaltenes, where 78 % residue is formed for the whole sample, approximately 60 % for the acetone as well as Tol/THF/MeOH fraction, and 64 % for the Hep/Tol fraction. It might be expected that the average mass loss of the measured solubility fractions equals to the mass loss of the whole asphaltene. However, all investigated fractions revealed a higher mass loss than unfractionated asphaltenes. This finding could support cooperative aggregation of asphaltenes from different solubility fractions forming highly stable aggregates which tend to coke formation rather than to volatize. Gray and co-workers demonstrated that model compounds can produce aggregates by π-π-stacking, which are thermally stable above 300 °C and show thermal degradation above 440 °C by coke formation. [73] Furthermore, highly polarizable compounds irreversibly bond to the silica gel during the fractionation process could additionally be associated with the higher coke residue of the whole asphaltene samples.

A fraction of the gas mixture evolved during TG measurements was investigated on-line by APCI-FT-ICR MS. The temperature resolved mass spectra given in Figure 3 provide an overview of the covered mass and temperature range. The total ion chromatogram (TIC) is overlaid in red. Comparison of the whole asphaltenes and their respective solvent fractions reveal remarkably different chemical profiles. As expected for the comparatively steep mass decrease of the TG curve of the whole asphaltenes, Athabasca and Wyoming asphaltenes reveal exclusively mass spectrometric response between 300-500 °C, with *m/z* up to 700 for Athabasca and *m/z* up to 600 for Wyoming asphaltenes. In earlier studies [33,44], we showed that purified asphaltenes exhibit TG and MS signal exclusively between 300-550 °C, when high-molecular weight structures are thermally cracked under pyrolysis conditions. Compounds desorbed intact below approximately 300 °C were regarded as occluded maltenes, co-precipitated within asphaltene aggregates [33]. For most of the solubility fractions, desorbable species also occur during 100-300 °C, and were not detected in the whole asphaltenes before. For Athabasca and Wyoming asphaltenes, the acetone fraction reveals the highest content of occluded material, indicating an enrichment of co-precipitated maltenes in this fraction. Athabasca asphaltenes show one apex during the desorption phase with a maximum *m/z* of 650, which starts at 100 °C and overlaps with the pyrolysis phase. Wyoming asphaltenes reveal two maxima for the desorption phase, the first between 150-230 °C with a mass range between m/z 150-450, and the second starting at 250 °C and overlapping with the pyrolysis phase ranging from *m/z* 200-550. It is important to point out that the initial extraction with acetone also aims to extract co-precipitated material that remained after heptane-washing in the standard preparation methods for asphaltene samples [74]. The Hep/Tol fraction of Athabasca asphaltenes covers a similar temperature and mass range as the whole sample. In contrast, Wyoming asphaltenes exhibit a low-abundant pattern during the desorption phase between 100-330 °C. The Tol/THF/MeOH fraction shows, for both asphaltenes, occluded material desorbed at elevated temperature and that overlaps with the actual pyrolysis phase. For this fraction, Athabasca asphaltenes reveal a higher content of occluded compounds, with most of the material having *m/z* values below 400, whereas Wyoming asphaltenes exhibit few compounds with *m/z* mostly below 300 in this fraction.

To investigate the chemical differences of the asphaltenes' building blocks and the occluded maltenes occurring in the different fractions, the time resolved mass spectra were separated into two individual phases. As separation temperature, the minimum of the TIC signal between of the desorbed compounds and the pyrolysis fragments is chosen. The separation temperatures slightly differ between the samples and are given for the individual fractions above the dashed lines in Figure 3. The slight shift in the separation temperature suggests variations in structural and chemical functionalities between the molecules involved in the desorption and pyrolysis processes. As pointed out, the molecular profiles of both phases overlaps to a certain extent making this approach partially artificial. Nevertheless, the desorption phase, up to 300-330 °C, is dominated by occluded material, whereas the pyrolysis phase is dominated by the asphaltene building blocks.

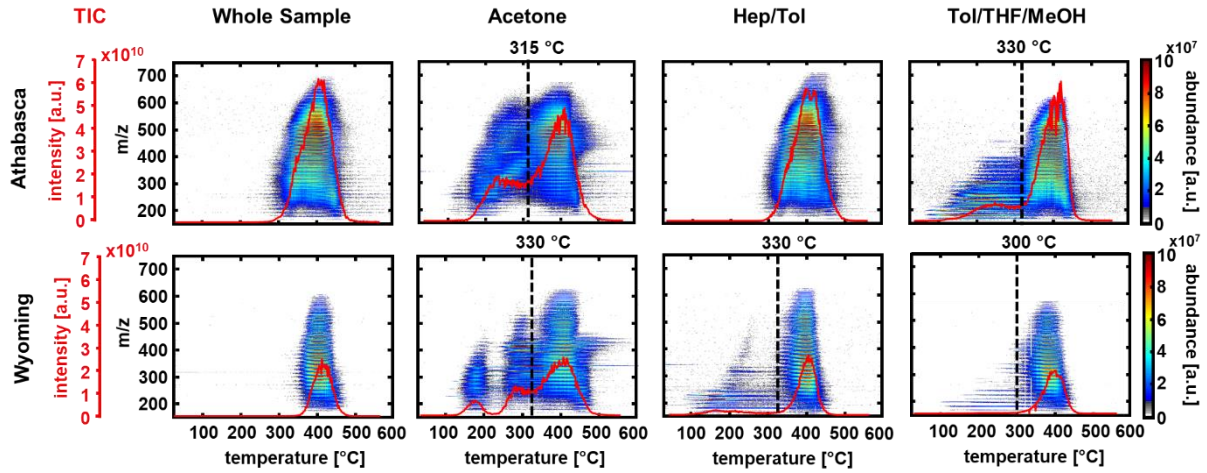

Figure 3: Survey view of the temperature-resolved mass spectra of Athabasca and Wyoming whole asphaltenes and their fractions. The TIC is overlaid in red. Fractions, which revealed occluded material during the desorption phase are separated at the minimum between desorption and pyrolysis phase.

Occluded Compounds

Due to extensive washing [50,52], the whole asphaltene samples do not reveal appreciable amounts of occluded compounds during thermal analysis [33,44]. Nonetheless, after the extrography fractionation, occluded compounds can be successfully exposed and seem to be enriched in several fractions, especially in the acetone fraction. The temperature profile of the TIC in Figure 3 of the desorbed compounds

indicates that those species are real occluded compounds and not low-molecular-weight asphaltenes. The TIC clearly exhibits a bimodal behavior, although both phases reveal an overlap for most of the fractions. If the species occurring in the desorption phase were low-molecular weight asphaltenes, they should reveal a continuous increase in boiling point in congruence with the Boduszynski continuum model [42,75–77], instead of the present pre-located distribution.

Figure 4 a) depicts the compound class distribution of the desorption phase for all samples of Athabasca and Wyoming asphaltenes. Athabasca asphaltenes showed intact desorbed occluded maltenes for the acetone and Tol/THF/MeOH fraction, while Wyoming asphaltenes revealed desorbable material for the acetone, Hep/Tol and Tol/THF/MeOH fraction. The acetone fraction exhibited for both asphaltenes the largest chemical diversity, covering the CH-, S1-, S2-, O1-, O2-, N1-, S1O1-, N1O1- and N1S1-classes. Athabasca asphaltenes acetone fraction additionally reveals a small content of occluded S3-class species. In comparison to the acetone fraction of the Wyoming asphaltenes, occluded material of Athabasca asphaltenes is enriched in CH-class and sulfur-containing classes, such as S1-S3, S1O1 and N1S1, whereas occluded compounds of Wyoming asphaltenes predominantly reveal CH-, O1 and O2-class species. The Wyoming Hep/Tol fraction also reveals occluded compounds mainly of CH-, O1- and O2-class species. Athabasca asphaltenes reveal a much higher content of occluded material in the Tol/THF/MeOH fraction than Wyoming asphaltenes. In this fraction, Athabasca asphaltenes are enriched in the CH-, O1- and O2-class indicating a higher content of polarizable functional groups, likely capable of interacting through hydrogen bonding with the actual asphaltene molecules. The few compounds occurring in the desorption phase of Wyoming asphaltenes Tol/THF/MeOH fraction predominantly belong to the CH-class.

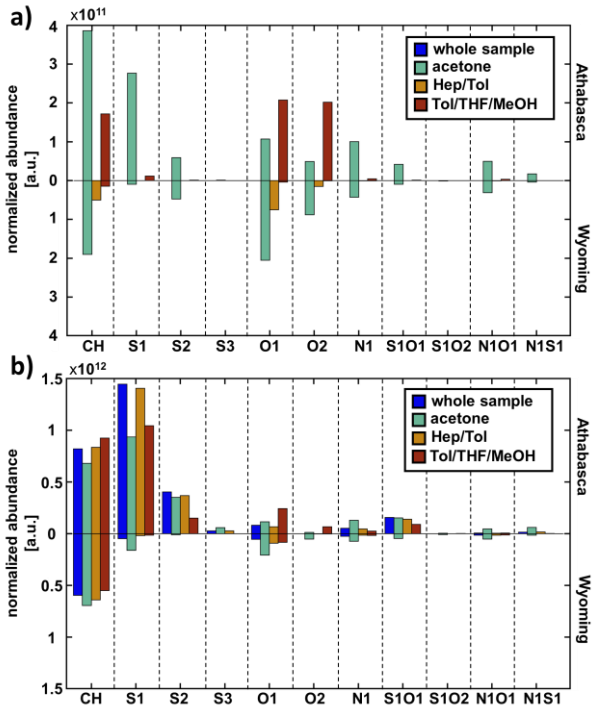

Figure 4: Overview on the normalized abundance of the compound classes of the whole asphaltenes and their solvent fractions for a) the desorption phase and b) the pyrolysis phase.

The occluded compounds vary not only in their absolute abundance between the two asphaltenes, they also differ in their compositional space. DBE versus #C-diagrams represent the compositional space by number of rings plus double bonds (DBE, y-axis) and molecular weight (carbon number, x-axis) and are presented in Figure 5 for the most abundant compound classes for the acetone and the Tol/THF/MeOH fractions. DBE versus #C diagrams for the Hep/Tol fraction of Wyoming asphaltenes are given in Figure S1 in the supplemental material. The blue line integrated in the DBE versus #C plots illustrates the planar aromatic hydrocarbon limit (PAH limit). The planar aromatic hydrocarbon limit is defined by the most compact PAHs, which are fused *peri*-condensed compounds [62–64]. These species are the most thermodynamically and kinetically stable. [63,78]

Acetone fraction. Acetone is known to extract occluded maltenes, low-molecular-weight asphaltenes, and asphaltene compounds with dominant island structure. [46,48,54,79] For both investigated asphaltenes, the extraction with acetone yielded the highest content of occluded material which features the

broadest compositional space in terms of compound class distribution and compositional space. For most of the compound classes, Athabasca asphaltenes reveal higher alkylation, whereas Wyoming occluded material exhibited mostly species clustering at the planar aromatic hydrocarbon limit (alky deficient). The CH-class of Athabasca asphaltenes occluded material reveals species with DBEs up to 20 and carbon numbers up to 47; with a maximum between 15 and 30 carbon atoms and DBEs below 10 as well as several, less alkylated compounds clustering at the aromatic limit. Wyoming asphaltenes reveal a lower proportion of CH-class compounds with an overall smaller covered compositional space with species up to 40 carbon atoms and a maximum between 15-25 and DBEs below 8. The O1-class is less abundant in Athabasca occluded compounds compared to Wyoming asphaltenes, but cover a slightly broader compositional space. Similar abundance trends are observed for the O2-class. Occluded nitrogen-containing species are abundant for the acetone fraction for both asphaltenes. Athabasca asphaltenes reveal predominantly N1-class species with DBEs between 9-20 and carbon numbers up to 40. Prominent species with DBEs 12 and 15 could tentatively be attributed to carbazoles [57,80] with one to two additional, condensed aromatic rings. Occluded Wyoming N1-compounds are comparatively less alkylated, with DBE 9, 12 and 15 as most prominent. N1O1-compounds reveal rather analogical behavior for both asphaltenes.

Athabasca asphaltenes are known to have a high concentration of sulfur-containing species [35]. The S1-class of occluded Athabasca compounds covers a broad compositional space with carbon numbers between 12-45 and DBEs up to 20. For this class, the abundance of low-DBE compounds with high alkylation and species clustering at the aromatic limit is quite equally distributed. Similar trend are observed for the S2- and S1O1-class with slightly lower maximum carbon numbers. Wyoming asphaltenes only reveal small amounts of occluded sulfur components. The S1- and S1O1-class exhibit mostly highly aromatic species with low alkylation. Interestingly and atypical compared to other compound classes, the S2-class only shows a small proportion of high aromatic species, whereas most of the compounds occur with DBEs between 4-11 and 15-35 carbon atoms. This comparatively high abundance of low-DBE, highly alkylated compounds suggests that the occluded S2-species in Wyoming asphaltenes are

more likely composed of two smaller, sulfur-containing cores linked by alkyl bridges rather than one highly aromatic core structure.

Hep/Tol fraction. Solely Wyoming asphaltenes exhibit occluded material in the Hep/Tol fraction with the CH-, O1- and O2-class as the most prominent compound classes. In Figure S1, the DBE versus #C diagram of the CH-class reveals species covering 15-40 carbon atoms with DBEs up to 15. Compounds with 10-20 carbons and DBEs 5-10 occur with higher abundance. The covered compositional space of the O1-class is much smaller. Occluded O1-class compounds are predominantly clustered at the PAH limit, with species consisting of 10-20 carbon atoms and abundant DBEs between 5 and 10. The O2-class reveals only a few compounds occurring in the maximum range of the O1-class.

Tol/THF/MeOH fraction. In contrast to the previously discussed fractions, the Tol/THF/MeOH fraction of Athabasca asphaltenes reveals a high content of occluded compounds clustering at the PAH limit with DBEs up to 20 and only a few compounds with low DBEs and high alkylation. However, Wyoming asphaltenes exhibit only minor amounts of occluded compounds, mostly represented in the CH- and O1-class with a narrow range of 13-17 carbon atoms and DBE values between 8-10. Since asphaltenes eluted with Tol/THF/MeOH were shown to be enriched in archipelago-type structural motifs [48], this result further supports Gray's hypothesis, that archipelago-type asphaltenes can easier occlude maltenes than island-type molecules [65]. In an earlier study, Athabasca asphaltenes were shown to be enriched in archipelago-type structures compared to Wyoming asphaltenes, which may explain the higher abundance of occluded material found in the Athabasca samples.

The CH-class of Athabasca asphaltenes occluded compounds contained highly abundant, aromatic species with 13-22 carbon atoms and DBE values of 8-15 as well as comparatively lower abundant compounds with 13-35 carbon atoms and DBEs below 7. The O1-, and particularly, the O2-class are shifted towards the planar aromatic limit. Although Wyoming asphaltenes are enriched in oxygen-containing occluded material (acetone and Hep/Tol fractions), they only exhibit small amounts of Ox species in the Tol/THF/MeOH-fraction, whereas Athabasca asphaltenes are enriched in O1- and O2-class species that concentrate in the most polarizable extrography fraction (Tol/THF/MeOH). Since the oxygen-species

occur in different solvent fractions with different polarity, it can be assumed that oxygen species present in the acetone and Hep/Tol fractions are less polarizable than species eluted by Tol/THF/MeOH. Thus, in the less polar fractions, oxygen might be contained as ketone-functionalities should be enriched, whereas highly polarizable fractions may contain hydroxyl- and carboxylic acid functionalities, capable of hydrogen bonding interactions with the silanol groups of the silica gel or polarizable asphaltene species. Strausz et al. (2006) summarized detailed investigations on occluded material obtained in the Soxhlet-extracted acetone fraction of Athabasca asphaltenes. [57] A series of ketones, carboxylic acids and minor amounts of alcohols was found by different analytical techniques [57], although the results are not completely comparable to the present study due to the lacking adsorption of the asphaltenes on silica gel prior to solvent treatment. In a more recent study, occluded compounds on asphaltenes were obtained by Soxhlet extraction with n-heptane and investigated by APPI-FT-ICR MS [52]. The highest polar fraction revealed CH-, O1-, S1- and N1-class species with low molecular weight compounds shifted towards the aromatic limit as well. It was concluded, that these compounds strongly interact with the asphaltene molecules by hydrogen bonding, acid-base interactions or pi-stacking due to high aromaticity. [52] Although the present asphaltenes underwent the same extensive washing process as the samples in the mentioned study, a small amount of strongly bonded compounds remain occluded within the asphaltene macrostructures and is released during the heating process of the thermobalance, indicating, that not all occluded material can be removed by washing with n-heptane.

Several works indicate that co-precipitates such as resins or aromatics are mostly composed of island-like structural motifs. [43,46] Regarding the observations within the different compound classes in this study, it can be concluded that occluded compounds can cover two different compositional spaces: The first region contains species with high aromaticity and short alkylation, while the other region is composed of compounds with lower DBE and higher carbon numbers. It depends on the compound class and the solubility fraction as well as the asphaltene origin, how pronounced the different regions are. For the CH-, O1-, S1-, S2- and S1O1-class both compositional regions are covered, while the N1- and N1O1-class only exhibit highly aromatic species. This bimodal distribution was also prior observed for

mid-polar fractions of occluded CH-, O1-, and S1-class compounds of a Colombian asphaltene. [52] Highly aromatic compounds with short alkylation were classified as “asphaltene-like” structures, while low-DBE compounds were classified as “maltene-like” structures, forming a compositional gap between both regions. [52] Furthermore, the results indicate that aggregation has large influences on the release of the occluded material during the heating process. In the whole asphaltene samples, the occluded compounds may be prevented from TG desorption by cooperative aggregation, which can explain the absence of species in the desorption phase. The acetone fraction was shown to have low aggregation potential [48], which prevents occlusion in aggregates and is consistent with the high amount of detected occluded material. These findings strengthen the idea of cooperative aggregation between asphaltene molecules of different fractions, which are partially separated during the extrography procedure.

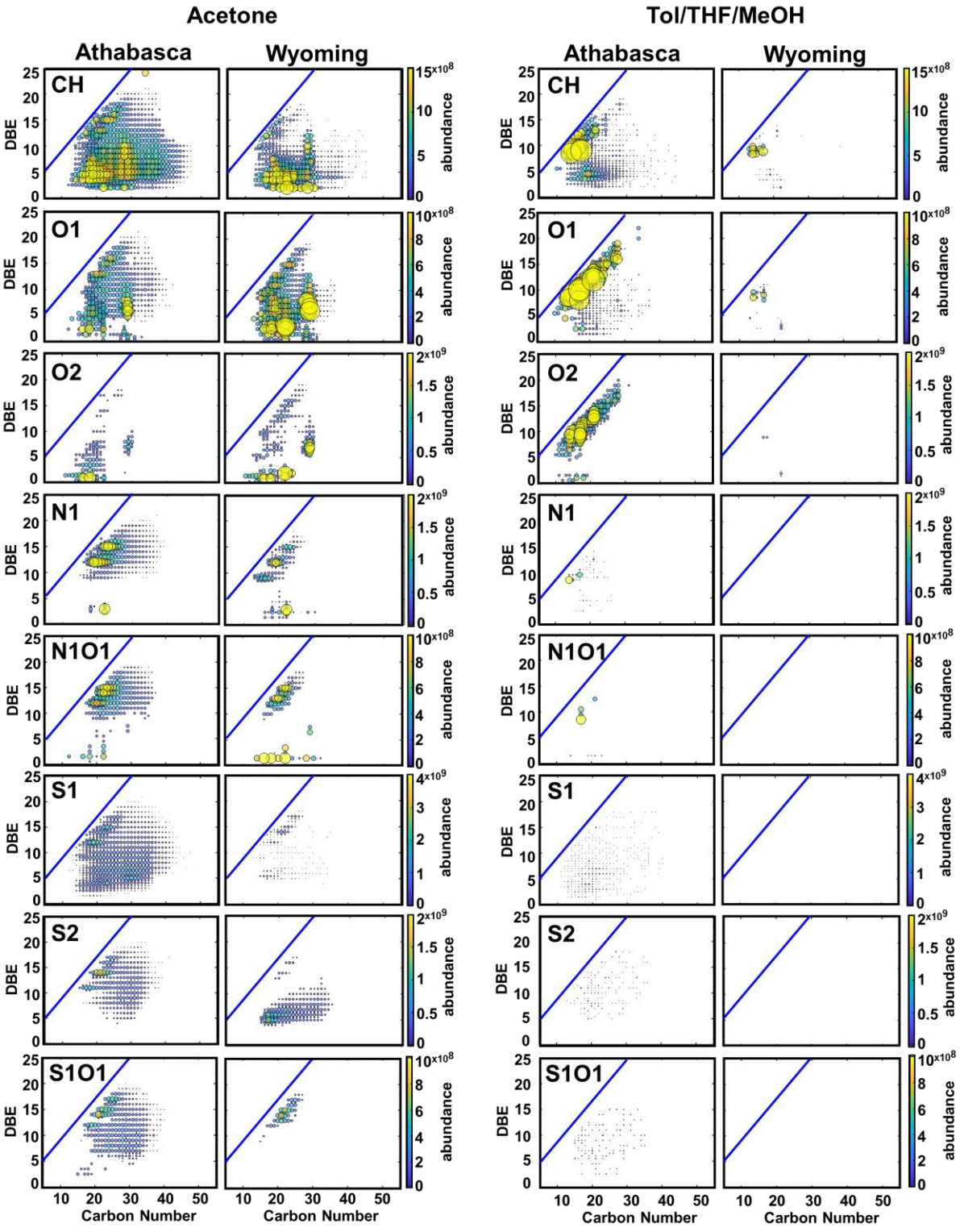

Figure 5: DBE vs. #C-plots summed over the desorption range of the TG-APCI-FT-ICR MS spectra for the acetone and Tol/THF/MeOH fraction of different compound classes occluded by Athabasca and Wyoming asphaltenes. The blue line indicates the planar aromatic limit.

Pyrolysis phase of the whole asphaltenes and their extrography fractions

The fractionation of crude oil derived material has been shown to provide great advantages in its molecular characterization by FT-ICR MS by increasing the number of attributed sum formulae and differentiating between chemical functionalities as well as structural motifs [81–84]. Although temperature-resolved evolved gas analysis already enables a thermal separation of the asphaltene matrix, additional fractionation increases the number of assigned compounds, which is depicted as Venn-diagrams in Figure 6. For Wyoming asphaltenes, a 2-fold increase of assigned molecular formulas is observed, whereas Athabasca asphaltenes reveal approximately a 1.5-fold increase of detected sum formulae. Regarding the extrographic fractions, the acetone fraction exhibited the highest amount of attributed sum formulae in both asphaltenes. This result further indicates the influence of aggregation on the thermal decomposition behavior of asphaltenes. Because of the low aggregation tendency of asphaltenes eluted with acetone, the non-aggregated asphaltenes could decompose more easily, which leads to the release of smaller, evaporable pyrolysis products. For fractions with high aggregation tendency, such as Tol/THF/MeOH, aggregates may prevent thermal decomposition and lead to coke formation instead.

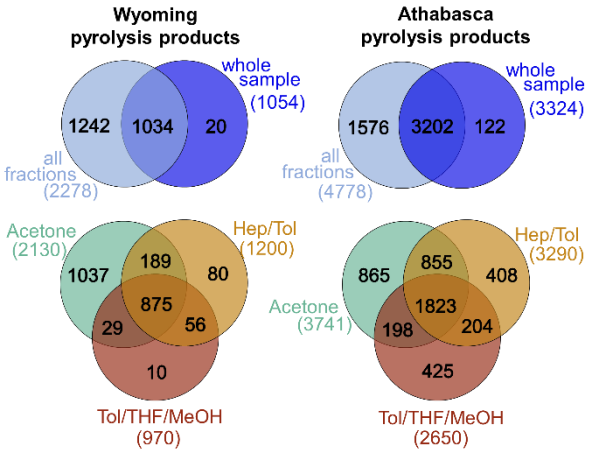

Figure 6: Venn diagrams of assigned sum formulae of Wyoming and Athabasca asphaltene pyrolysis products as well as their solubility fractions.

In Figure 4 b) the compound class distribution of the pyrolysis phase is presented. While the occluded material mostly covers specific compound classes only, the asphaltene pyrolysis products were found

for all main compound classes. Athabasca asphaltenes pyrolysis products cover the CH-, S1-, S2-, S3-, O1-, O2-, N1-, S1O1-, S1O2-, N1O1- and N1S1-class, which account together for 97 to 100 % of the total assigned absolute abundance. Pyrolysis products of Wyoming asphaltenes reveal mainly the same compound classes except for the S2- and S3-class, which account together for 99-100 % of the total assigned absolute abundance. At first glance, the revealed compound classes exhibit unsuspected low complexity compared to direct infusion studies. However, the detected compounds are pyrolysis fragments of the asphaltenes showing probably reduced complexity because of pyrolytic cracking. If a poly-heteroatomic multicore asphaltene, which contains heteroatoms in several cores, is cracked, the remaining fragments will occur in different compound classes. Regarding single core asphaltenes, poly-heteroatomic asphaltenes most likely cleave of alky side chains leaving the core intact. In Figure 7, examples are presented for both types of asphaltenes. On the left side, a possible structure for a single core asphaltene of the N1S1-class is shown. After thermal cracking and cleavage of the side chains, the aromatic core remains in the N1S1-class. In contrast, a possible multi core asphaltene of the N1S1-class shown on the right side is likely to be cracked into two smaller core structures. If the heteroatoms are present in different cores, the fragments will occur in the N1-class and S1-class, with respect to the presented example. This type of thermal degradation might give rise to mono-heteroatomic compound classes. Similar trends were previously observed by investigating the compositional changes of asphaltenes during thermal cracking and hydroconversion by direct infusion APPI-FT-ICR MS [34]. The maltene fraction obtained by cracking was shown to contain only 9 major compound classes, while the parent asphaltenes consisted of 21 classes [34].

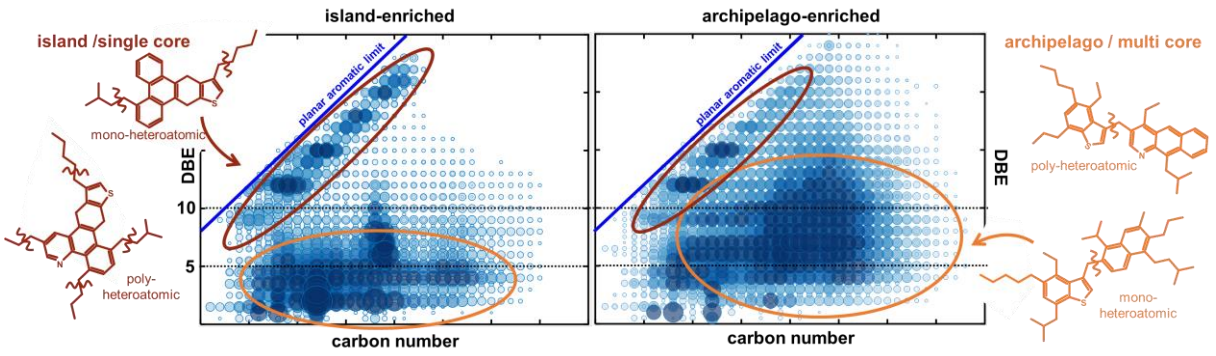

Figure 7: Exemplary DBE versus #C diagram of the pyrolysis phase with all compound classes overlaid for island-enriched (Wyoming) and archipelago-enriched (Athabasca) asphaltenes. Two distinct regions are revealed, in which pyrolysis fragments are observed with high abundance. The first region is observed for species clustering at the aromatic limit with comparatively high DBE values. Those pyrolysis fragments are most likely derived from island-like asphaltenes cleaved of alkyl side chains or smaller pendant groups leaving the aromatic core intact. The second region is observed at low DBE values and higher carbon numbers. Those pyrolysis fragments most likely are derived from the cleavage of multi core/ archipelago-type asphaltenes and small pendant groups from island structural motifs. Multi cores are preferentially cracked at their bridges, which reduces the DBE value. Nonetheless, alkyl side chains are mostly preserved, therefore, those pyrolysis fragments occur at comparatively high carbon numbers.

By investigating the DBE versus #C diagrams of asphaltenes decomposed during pyrolysis, two distinct regions of high abundant thermal fragments become apparent. Figure 7 provides exemplary DBE vs. #C diagrams for the pyrolysis phase of the acetone fraction of an island-enriched asphaltene (Wyoming) and an archipelago-enriched asphaltene (Athabasca). All compound classes are overlaid. The first region is observed for thermal fragments with high DBE-values and low carbon numbers indicating low alkylation, which cluster near the planar aromatic hydrocarbon limit. Those pyrolysis fragments are most likely derived from the thermal decomposition of island-type / single core asphaltenes cleaving off alkyl side chains as well as small pendant groups and leaving the aromatic cores intact. Island-enriched asphaltenes are more pronounced in this region than archipelago-enriched asphaltenes. The second region is observed for lower DBE values and comparatively high carbon numbers. Island-enriched asphaltenes are in this region enriched in pyrolysis fragments with DBE values below 5. This finding indicates that the observed fragments derive from alkyl side chains, which might contain small naphthenic or phenylic pendant groups, cleaved of during pyrolysis. Archipelago-enriched asphaltenes reveal only a minor amount of exceptionally low DBE-species. However, those asphaltenes exhibit high abundant signal for

thermal fragments with DBE values between 4 and 15. These species are likely to be derived from archipelago / multi core asphaltenes, which are preferentially cracked at linkers bridging the aromatic cores, which decreases the DBE values. Due to preserving the alkyl side chains, those thermal decomposition products occur at comparatively high carbon numbers. However, also side reactions between radicals formed during pyrolysis could generate species with high carbon numbers.

In Figure 8, DBE vs. #C plots of the four most abundant compound classes in both asphaltenes, namely the CH-, O1-, S1- and N1-class, are presented. The covered compositional space of the shown classes is comparable to the maltene fraction of thermal upgrading products of Colombian asphaltenes investigated by DI-APPI-FT-ICR MS [34]. Especially, the CH-class with high abundant low-DBE compounds and the N-class with species abundant for DBE 9 and higher reveal great similarity between both studies. Regarding the whole asphaltenes compared to their extrography fractions, the samples differ in the covered compositional space. For Athabasca asphaltenes, the compositional space of the whole asphaltene sample is quite similar to the Hep/Tol fraction, while Wyoming asphaltenes revealed similarity to the Hep/Tol and Tol/THF/MeOH fraction. These findings differ from results revealed by direct infusion FT-ICR MS, where the acetone fraction was shown to mainly equal the whole asphaltene sample [48]. Acetone was found to elute compounds with high monomeric ion yield due to its sufficient solvation ability of small, peri-condensed aromatic hydrocarbons [48], such as highly occluded material and low molecular weight, island-like asphaltenes [14,79,85,86]. These findings led to the assumption that mass spectrometry, assisted by atmospheric pressure photoionization (APPI), reflects mainly the components with the highest monomer ion yield [48]. For the TG-FT-ICR MS coupling applied in his study, comparatively strong matrix effects caused by the acetone fraction were not observed, because TG provides a separation of the compounds by their thermal behavior, which partially overcomes matrix effects observed for direct infusion techniques.

As depicted in Figure 8 a), whole Athabasca asphaltenes reveal pyrolysis fragments with DBEs up to 20 and carbon numbers up to 50 for the CH-class, with species below DBE 10 as most prevalent. A substantial amount of high abundant compounds was also observed below the aromatic boundary of DBE 4.

These compounds most probably correspond to alkenes produced by thermal cracking of alkyl side chains [87] as well as building blocks containing naphthenic structural elements [25,32,55]. Wyoming whole asphaltenes revealed a lower maximum DBE of 16 and carbon numbers up to 45, with high amounts of non- or low-aromatic CH-class pyrolysis fragments detected. The non- or low-aromatic fragments most probably are derived from the cleavage of small naphthenic or even aromatic pendant groups or alkyl side chains, forming alkenes by hydrogen abstraction [87] due to the thermal cracking process. Considering that Wyoming asphaltenes are enriched in island structural motifs compared to Athabasca asphaltenes, the higher abundance of species with DBE 4 or lower can be explained by the afore-mentioned thermal degradation reaction. This difference between both asphaltenes in the CH-class is observed for all fractions. Furthermore, at first glance, the higher maximum DBE of the CH-class observed for species clustering at the aromatic limit in whole Athabasca asphaltenes and all fractions compared to the Wyoming asphaltene equivalents contradicts the fact that Wyoming asphaltenes are enriched in highly aromatic, island-type structures. However, due to the high TGA residue of Wyoming asphaltenes, which composition was not accessed in this study, it can be assumed that these asphaltenes contain high amounts of compounds with large aromatic, island-like cores serving as coke precursors. Athabasca asphaltenes, however, seem to contain smaller island-type structures, which are still evaporable after cleaving off the alkyl side chains during the pyrolysis process.

The acetone fraction differs the most from the other fractions revealing a bimodal distribution of island- and archipelago-type pyrolysis products. Comparable to that, McKenna et al. (2019) observed a bimodal distribution by distillation of high petroleum boiling cuts, which was suggested to be derived from thermal cracking of archipelago-type compounds and the detection of island-type structures [10]. In this study, both asphaltene samples exhibit, for the CH-class, pyrolysis fragments with higher DBE values: up to 25 for Athabasca bitumen asphaltenes and up to 23 for Wyoming asphaltenes. Nonetheless, Athabasca asphaltenes revealed the highest abundance for building blocks with DBE below 15 and 15-45 carbon atoms, whereas Wyoming asphaltenes are enriched in highly aromatic building blocks (DBE 10-23) clustering at the aromatic limit. The comparatively high amount of high aromatic species can be

explained by the property of acetone to extract asphaltene compounds with single-core structure, which exhibit a weaker aggregation tendency [48,85,86]. Recently, it was shown that the dominance of island and archipelago structural motifs depends not only on the geological origin of asphaltenes but also on the molecular weight [50]. Lower *m/z*-values and therefore, low-molecular weight asphaltenes, were found to be enriched in island structural motifs, whereas high m/z-values revealed both motif types [50]. As Wyoming asphaltenes contain high amounts of island-like structures, also low-molecular weight asphaltenes seem to be enriched in compounds with highly aromatic, condensed cores. Besides the acetone fraction, also the Tol/THF/MeOH fraction reveals differences to the whole sample; the differences are more pronounced for Athabasca asphaltenes. Compared to the other fractions, low-DBE CH-compounds revealed lower alkylation. Furthermore, pyrolysis products with DBEs between 10-15 are comparatively enriched in the Tol/THF/MeOH-fraction, indicating a correlation with the aromatic character and therefore polarity of the compounds eluted in this fraction.

Not only the CH-class exhibit differences between the whole asphaltenes and their fractions, heteroatom-containing compound classes differ in their compositional space as well. Figure 8 b) shows DBE vs. #C diagrams of the O1-class. In both whole asphaltenes, only minor amounts of oxygen-containing components are detected in the pyrolysis phase. During thermal decomposition, highly polarizable oxygen-containing functionalities could be cleaved off, and more thermally stable oxygen compounds, such as ketones, are mostly detected. For Athabasca asphaltenes, the O1-class is enriched in the acetone and Tol/THF/MeOH-fraction, while Wyoming asphaltenes only exhibit higher amounts of oxygen-containing compounds in the acetone fraction. As already revealed for the CH-class, both asphaltenes showed in the acetone fraction a distinct bimodal distribution of island-like and archipelago-like pyrolysis fragments. Highly aromatic pyrolysis products, clustering at the aromatic limit, were detected with DBE values between 10-25, while species with higher alkylation, with up to 35-40 carbon atoms, reached DBEs not higher than 15. Specifically, Wyoming asphaltenes revealed a high enrichment in island-like O1-class compounds; but also, higher alkylated species with lower DBEs exhibit a second maximum in absolute abundance. For Athabasca asphaltenes, highly aromatic O1-class fragments are less pronounced in the

acetone fraction. However, as observed for occluded material, highly aromatic species with DBEs between 12-20 are enriched in the Tol/THF/MeOH-fraction indicating a higher polarity of the oxygen-containing functionalities compared to those occurring in the acetone fraction. This observation is supported by Frakman et al. (1990), who revealed less polar ketones, such as fluorenones (DBE 9) and benzofluorenones (DBE 12), in high quantities in the acetone fraction of Athabasca asphaltenes [79]. Moreover, Nascimento et al. (2016) reported a high content of polar functionalities, such as basic nitrogen, carboxylic groups or ketones, in THF-eluted fractions [24], supporting the findings for the highly aromatic Athabasca pyrolysis products. Besides, in the THF/MeOH fraction of South American Medium asphaltenes and the Petrophase-2017 asphaltene, a high O/C-ratio was revealed by APPI-FT-ICR MS, as reported by Rodgers et al. [48]. The authors demonstrated that direct infusion experiments on the same asphaltene samples revealed an enrichment of highly aromatic oxygen-containing compounds for Wyoming asphaltenes [50]. With the TG-FT-ICR MS approach, these species were not accessible, although they should have been ionized by APCI. Thus, we hypothesize that these highly polarizable/ aromatic compounds were remained in the residue during the heating process.

Compared to Wyoming asphaltenes, sulfur-containing compounds are more pronounced in Athabasca building blocks, which is demonstrated by the high absolute abundance (Figure 4) and number of assigned sum formulae (Figure S2) of the S1- to S3-class as well as the S1O1-class. In contrast to the occluded compounds of Athabasca asphaltenes, where sulfur species were highly enriched in the acetone fraction, sulfur-containing pyrolysis products were detected with higher absolute abundance in the whole asphaltene and in the Hep/Tol fraction. At the molecular level, differences in the prevalence of structural motifs are observed for both asphaltenes. In the whole sample, S1-class pyrolysis products of Athabasca asphaltenes cover a broad compositional space with up to DBE 22 and 48 carbon atoms. Predominant structural motives feature archipelago-type character due to DBE values below 12 and high absolute abundance for carbon numbers between 20-40. Wyoming asphaltenes only exhibited a limited compositional space of species with higher abundance between DBE 9-15 and short alkylation. For the Wyoming asphaltenes, especially building blocks with DBE 9 and 12 are prevalent, which can

tentatively be attributed to dibenzothiophenes and benzonaphthothiophenes [31,35,55]. In the acetone fraction, S1-class pyrolysis fragments revealed higher DBE values with DBEs up to 25 for Athabasca asphaltenes and up to 23 for Wyoming asphaltenes. In this fraction, Wyoming asphaltenes are clearly enriched in highly aromatic structures, while Athabasca asphaltenes are shifted to lower DBEs with higher alkylation. Remarkably, Athabasca asphaltenes eluted with acetone show only low abundance for S1-compounds with DBEs less than 6 (tentatively benzothiophenes [76]), which is different to all other samples. The Tol/THF/MeOH-fraction, however, is enriched in low-DBE S1-class species with DBE 2 as most prominent. In the literature, low-DBE sulfur compounds have been attributed to sulfides, thiolanes and thianes [88,89]. Similar was observed for the Petrophase-2017 asphaltene, where the THF fraction exhibited higher alkylated compounds with low DBEs as well [48].

The N1-class of the pyrolyzed asphaltenes in Figure 8 d) revealed similar main features as previously discussed for the other compound classes. Athabasca asphaltenes exhibited for all fractions predominantly N1-class species with DBEs greater than 10. In the acetone fraction, a bimodal behavior of island- and archipelago-related structures is observed, which is quite balanced between both structural motifs. For this fraction, Wyoming asphaltenes stand in strong contrast to the Athabasca sample. Except for some low abundant pyrolysis products with small DBEs, Wyoming asphaltenes only exhibit high aromatic, island-like structural motifs clustering at the aromatic limit. Other fractions and the whole asphaltene sample mostly exhibit non- to low aromatic pyrolysis products with DBEs less than 6. This dominant difference between the acetone fraction of Athabasca and Wyoming asphaltenes with regard to the structural motifs is observed for the S1O1-, N1O1 and N1S1-class as well, for which the DBE vs. #C diagrams are given in the supplemental material in Figure S3.

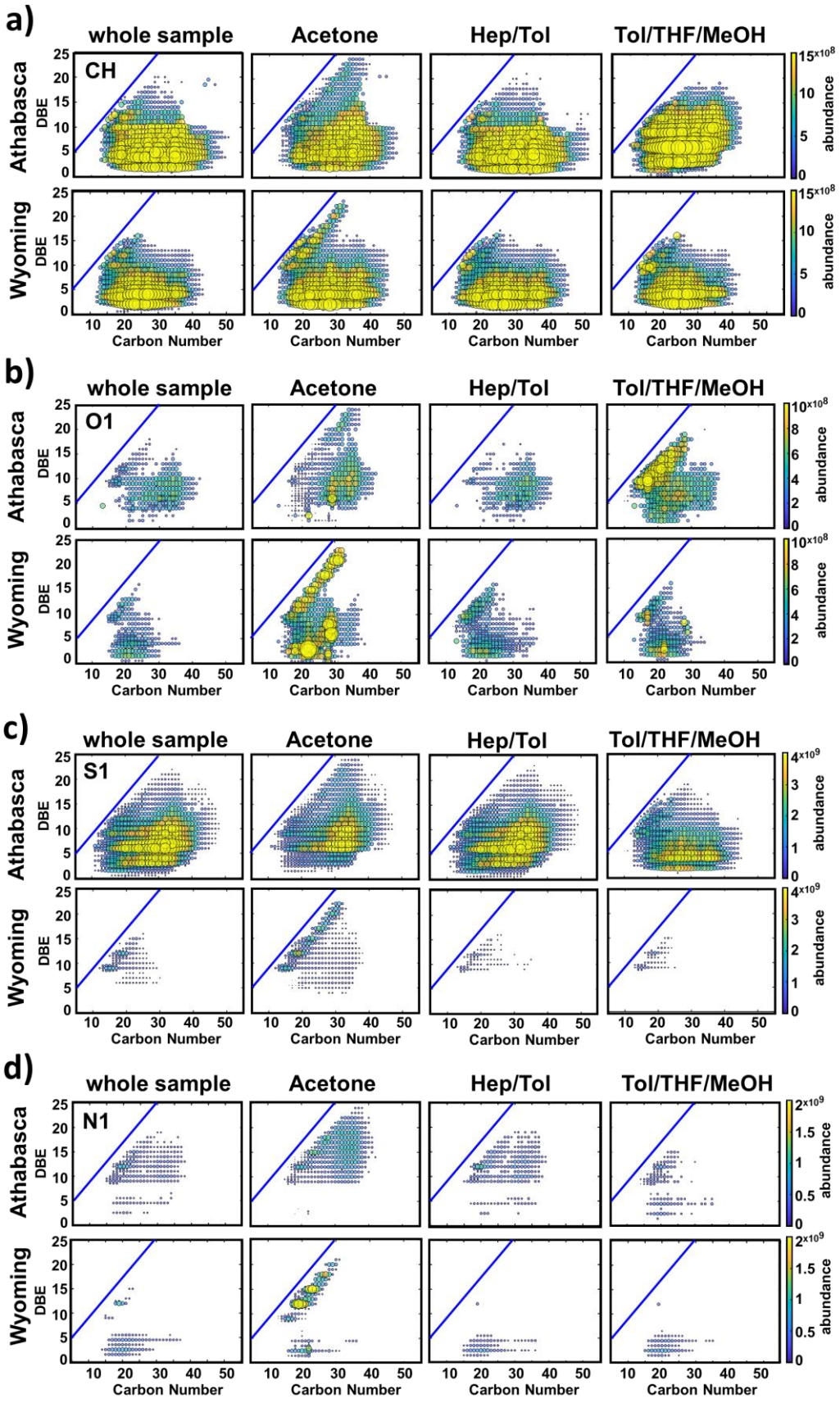

Figure 8: DBE versus #C diagrams of the pyrolysis fragments of Athabasca and Wyoming whole asphaltenes and their fractions measured by TG-APCI-FT-ICR MS: a) CH-class, b) O1-class, c) S1-class and d) N1-class. . The blue line indicates the planar aromatic limit.

The bimodal behavior of island-type and archipelago-type asphaltenes, which was predominant in the acetone fraction for TG-FT-ICR MS, is comparable to observations made by IRMPD-APPI-FT-ICR MS in the literature [46,48,50]. IRMPD fragmentation is based on the uptake of IR-photons by vibration states (thermal activation) of gas phase ions in high vacuum leading to their fragmentation [90]. To a certain extent, IRMPD can be compared to the thermal cracking that occurs during evolved gas analysis, where molecules are thermally decomposed in liquid/ solid phase under atmospheric pressure with potential molecular interactions. However, it is interesting to note that both techniques provide consistent molecular profiles for asphaltene samples composed of island and archipelago motifs: It was shown for IRMPD, that island-type structural motifs cleave of their side chains, which results in similar DBE values but a reduction in carbon number shifting the fragments toward the planar aromatic limit [46,48]. Archipelago-type asphaltenes exhibited an apparent decrease in DBE and carbon number in comparison to the precursor ions in IRMPD [46,48]. In this study, we revealed that thermal analysis provides results consistent with bulk thermal decomposition, since island enriched samples yield a higher amount of coke/highly aromatic core structures, whereas archipelago-type asphaltenes yield maltenes/low DBE pyrolysis products. Archipelago-type structural motifs were characterized by low-DBE values and a broad carbon number distribution. This result differs from IRMPD, where archipelago fragments are also fragmented down to their core structures, because the thermal decomposition under atmospheric pressure enables collisional cooling preserving the alkyl chains. On the contrary, island-type structures showed highly dealkylated, highly aromatic pyrolysis fragments clustering at the planar aromatic limit and revealed a higher coke formation tendency. Therefore, TG-FT-ICR MS provides an additional technique to investigate the predominant structures in asphaltenes by combining the amount of TGA residue and thermal cracking fragments.

Conclusion

In this study, two asphaltenes, one is enriched in island-type structural motifs (Wyoming asphaltenes) and one in archipelago-type structural motifs (Athabasca asphaltenes), as well as their extrography fractions were investigated by TG-APCI-FT-ICR MS. During desorption up to a temperature of ca. 300 °C, occluded material was desorbed intact, whereas during the pyrolysis process, thermal fragments of the asphaltenes were detected. The following main conclusions could be revealed by analysing the thermal decomposition products of the different asphaltenes:

(1) Island-enriched asphaltenes yield higher coke residues than archipelago-enriched asphaltenes.
(2) Whole asphaltenes were found to yield higher amounts of TGA residue than their solubility fractions, which is assumed to be caused by highly polar compounds not eluted during the fractionation process as well as cooperative aggregation between asphaltene molecules of different polarity.
(3) Although the asphaltenes were extensively washed, highly occluded material was revealed particularly in the acetone and Tol/THF/MeOH-fraction indicating partially separation of cooperative aggregates.
(4) A bimodal behavior was revealed for most of the compound classes of the pyrolysis fragments, representing the presence of archipelago- and island-type structural motifs in both asphaltenes. The bimodal distribution was most prevalent in the acetone fraction. Especially for the O1-class of Athabasca bitumen, the prevalent structural motif depended on the solubility fraction.
(5) Pyrolysis products with high DBE and short alkylation are likely to originate from island-type asphaltenes, whereas pyrolysis products with low DBE-values and high carbon numbers may derive from archipelago-type asphaltenes.

TG-API-FT-ICR MS was shown to successfully address the structural motif debate of asphaltenes. By combining the mass loss information with the molecular fingerprint in terms of characteristic areas in DBE versus #C diagrams for island- and archipelago-type motifs, comparable characteristic shifts

could be revealed as shown for DI-IRMPD-FT-ICR MS. Therefore, TG-FT-ICR MS provides a corresponding molecular resolving approach, which cannot be achieved by microscopic, spectroscopic or even low-resolution pyrolysis techniques. Future studies will focus on the extremely polarizable, irreversibly bonded asphaltene material during extrography fractionation with TG-FT-ICR MS.

Acknowledgement

A portion of the work presented herein was performed at the National High Magnetic Field Laboratory ICR User Facility, which is supported by the National Science Foundation Division of Chemistry through Cooperative Agreement DMR-1644779, and the State of Florida. Funding by the Horizon 2020 program for the EU FT-ICR MS project (European Network of Fourier-Transform Ion-Cyclotron-Resonance Mass Spectrometry Centers, Grant agreement ID: 731077) is gratefully acknowledged. The authors thank the German Research Foundation (DFG) for funding of the Bruker FT-ICR MS (INST 264/56).

References

1. Adams, J.J. Asphaltene Adsorption, a Literature Review. *Energy Fuels* 2014, *28*, 2831–2856, doi:10.1021/ef500282p.
2. Akbarzadeh, K.; Hammami, A.; Kharrat, A.; Zhang, D.; Allenson, S.; Creek, J.; Kabir, S.; Jamaluddin, A.J.; Marshall, A.G.; Rodgers, R.P.; et al. Asphaltenes—Problematic but Rich in Potential. *Oilfield Review* 2007, 22–43.
3. Buckley, J.S. Asphaltene Deposition. *Energy Fuels* 2012, *26*, 4086–4090, doi:10.1021/ef300268s.
4. Hammami, A.; Ratulowski, J. Precipitation and Deposition of Asphaltenes in Production Systems: A Flow Assurance Overview. In *Asphaltenes, heavy oils and petroleomics*; Mullins, O.C., Ed.; Springer: New York, NY, 2007; pp 617–660, ISBN 978-0-387-31734-2.
5. Moulijn, J.A.; van Diepen, A.E.; Kapteijn, F. Catalyst deactivation: is it predictable? *Applied Catalysis A: General* 2001, *212*, 3–16, doi:10.1016/S0926-860X(00)00842-5.
6. Palacio Lozano, D.C.; Thomas, M.J.; Jones, H.E.; Barrow, M.P. Petroleomics: Tools, Challenges, and Developments. *Annu. Rev. Anal. Chem. (Palo Alto Calif)* 2020, *13*, 405–430, doi:10.1146/annurev-anchem-091619-091824.
7. Schuler, B.; Meyer, G.; Peña, D.; Mullins, O.C.; Gross, L. Unraveling the Molecular Structures of Asphaltenes by Atomic Force Microscopy. *J. Am. Chem. Soc.* 2015, *137*, 9870–9876, doi:10.1021/jacs.5b04056.
8. Schuler, B.; Fatayer, S.; Meyer, G.; Rogel, E.; Moir, M.; Zhang, Y.; Harper, M.R.; Pomerantz, A.E.; Bake, K.D.; Witt, M.; et al. Heavy Oil Based Mixtures of Different Origins and Treatments Studied by Atomic Force Microscopy. *Energy Fuels* 2017, *31*, 6856–6861, doi:10.1021/acs.energyfuels.7b00805.
9. Panda, S.K.; Andersson, J.T.; Schrader, W. Characterization of supercomplex crude oil mixtures: what is really in there? *Angewandte Chemie International Edition* 2009, *48*, 1788–1791, doi:10.1002/anie.200803403.

10. McKenna, A.M.; Chacón-Patiño, M.L.; Weisbrod, C.R.; Blakney, G.T.; Rodgers, R.P. Molecular-Level Characterization of Asphaltenes Isolated from Distillation Cuts. *Energy Fuels* 2019, *33*, 2018–2029, doi:10.1021/acs.energyfuels.8b04219.

11. Calemma, V.; Rausa, R.; D'Anton, P.; Montanari, L. Characterization of Asphaltenes Molecular Structure. *Energy Fuels* 1998, *12*, 422–428, doi:10.1021/ef9701854.

12. Payzant, J.D.; Lown, E.M.; Strausz, O.P. Structural units of Athabasca asphaltene: the aromatics with a linear carbon framework. *Energy Fuels* 1991, *5*, 445–453, doi:10.1021/ef00027a015.

13. McKenna, A.M.; Donald, L.J.; Fitzsimmons, J.E.; Juyal, P.; Spicer, V.; Standing, K.G.; Marshall, A.G.; Rodgers, R.P. Heavy Petroleum Composition. 3. Asphaltene Aggregation. *Energy Fuels* 2013, *27*, 1246–1256, doi:10.1021/ef3018578.

14. Putman, J.C.; Moulian, R.; Barrère-Mangote, C.; Rodgers, R.P.; Bouyssiere, B.; Giusti, P.; Marshall, A.G. Probing Aggregation Tendencies in Asphaltenes by Gel Permeation Chromatography. Part 1: Online Inductively Coupled Plasma Mass Spectrometry and Offline Fourier Transform Ion Cyclotron Resonance Mass Spectrometry. *Energy Fuels* 2020, *34*, 8308–8315, doi:10.1021/acs.energyfuels.0c01522.

15. Pinkston, D.S.; Duan, P.; Gallardo, V.A.; Habicht, S.C.; Tan, X.; Qian, K.; Gray, M.; Müllen, K.; Kenttämaa, H.I. Analysis of Asphaltenes and Asphaltene Model Compounds by Laser-Induced Acoustic Desorption/Fourier Transform Ion Cyclotron Resonance Mass Spectrometry. *Energy Fuels* 2009, *23*, 5564–5570, doi:10.1021/ef9006005.

16. Pomerantz, A.E.; Hammond, M.R.; Morrow, A.L.; Mullins, O.C.; Zare, R.N. Two-step laser mass spectrometry of asphaltenes. *J. Am. Chem. Soc.* 2008, *130*, 7216–7217, doi:10.1021/ja801927v.

17. Pomerantz, A.E.; Hammond, M.R.; Morrow, A.L.; Mullins, O.C.; Zare, R.N. Asphaltene Molecular-Mass Distribution Determined by Two-Step Laser Mass Spectrometry †. *Energy Fuels* 2009, *23*, 1162–1168, doi:10.1021/ef8006239.

18. Groenzin, H.; Mullins, O.C. Molecular Size and Structure of Asphaltenes from Various Sources. *Energy Fuels* 2000, *14*, 677–684, doi:10.1021/ef990225z.

19. Hurt, M.R.; Borton, D.J.; Choi, H.J.; Kenttämaa, H.I. Comparison of the Structures of Molecules in Coal and Petroleum Asphaltenes by Using Mass Spectrometry. *Energy Fuels* 2013, *27*, 3653–3658, doi:10.1021/ef302024z.

20. Yen, T.F.; Erdman, J.G.; Pollack, S.S. Investigation of the Structure of Petroleum Asphaltenes by X-Ray Diffraction. *Anal. Chem.* 1961, *33*, 1587–1594, doi:10.1021/ac60179a039.

21. Mullins, O.C. The Modified Yen Model †. *Energy Fuels* 2010, *24*, 2179–2207, doi:10.1021/ef900975e.

22. Schuler, B.; Zhang, Y.; Collazos, S.; Fatayer, S.; Meyer, G.; Pérez, D.; Guitián, E.; Harper, M.R.; Kushnerick, J.D.; Peña, D.; et al. Characterizing aliphatic moieties in hydrocarbons with atomic force microscopy. *Chem. Sci.* 2017, *8*, 2315–2320, doi:10.1039/c6sc04698c.

23. Zhang, Y.; Schuler, B.; Fatayer, S.; Gross, L.; Harper, M.R.; Kushnerick, J.D. Understanding the Effects of Sample Preparation on the Chemical Structures of Petroleum Imaged with Noncontact Atomic Force Microscopy. *Ind. Eng. Chem. Res.* 2018, *57*, 15935–15941, doi:10.1021/acs.iecr.8b03962.

24. Nascimento, P.T.H.; Santos, A.F.; Yamamoto, C.I.; Tose, L.V.; Barros, E.V.; Gonçalves, G.R.; Freitas, J.C.C.; Vaz, B.G.; Romão, W.; Scheer, A.P. Fractionation of Asphaltene by Adsorption onto Silica and Chemical Characterization by Atmospheric Pressure Photoionization Fourier Transform Ion Cyclotron Resonance Mass Spectrometry, Fourier Transform Infrared Spectroscopy Coupled to Attenuated Total Reflectance, and Proton Nuclear Magnetic Resonance. *Energy Fuels* 2016, *30*, 5439–5448, doi:10.1021/acs.energyfuels.6b00523.

25. Artok, L.; Su, Y.; Hirose, Y.; Hosokawa, M.; Murata, S.; Nomura, M. Structure and Reactivity of Petroleum-Derived Asphaltene. *Energy Fuels* 1999, *13*, 287–296, doi:10.1021/ef980216a.

26. Sabbah, H.; Morrow, A.L.; Pomerantz, A.E.; Mullins, O.C.; Tan, X.; Gray, M.R.; Azyat, K.; Tykwinski, R.R.; Zare, R.N. Comparing Laser Desorption/Laser Ionization Mass Spectra of Asphaltenes and Model Compounds. *Energy Fuels* 2010, *24*, 3589–3594, doi:10.1021/ef100402g.

27. Sabbah, H.; Morrow, A.L.; Pomerantz, A.E.; Zare, R.N. Evidence for Island Structures as the Dominant Architecture of Asphaltenes. *Energy Fuels* **2011**, *25*, 1597–1604, doi:10.1021/ef101522w.

28. Tang, W.; Hurt, M.R.; Sheng, H.; Riedeman, J.S.; Borton, D.J.; Slater, P.; Kenttämaa, H.I. Structural Comparison of Asphaltenes of Different Origins Using Multi-stage Tandem Mass Spectrometry. *Energy Fuels* **2015**, *29*, 1309–1314, doi:10.1021/ef501242k.

29. Riedeman, J.S.; Kadasala, N.R.; Wei, A.; Kenttämaa, H.I. Characterization of Asphaltene Deposits by Using Mass Spectrometry and Raman Spectroscopy. *Energy Fuels* **2016**, *30*, 805–809, doi:10.1021/acs.energyfuels.5b02002.

30. Borton, D.; Pinkston, D.S.; Hurt, M.R.; Tan, X.; Azyat, K.; Scherer, A.; Tykwinski, R.; Gray, M.; Qian, K.; Kenttämaa, H.I. Molecular Structures of Asphaltenes Based on the Dissociation Reactions of Their Ions in Mass Spectrometry. *Energy Fuels* **2010**, *24*, 5548–5559, doi:10.1021/ef1007819.

31. Rueda-Velásquez, R.I.; Freund, H.; Qian, K.; Olmstead, W.N.; Gray, M.R. Characterization of Asphaltene Building Blocks by Cracking under Favorable Hydrogenation Conditions. *Energy Fuels* **2013**, *27*, 1817–1829, doi:10.1021/ef301521q.

32. Karimi, A.; Qian, K.; Olmstead, W.N.; Freund, H.; Yung, C.; Gray, M.R. Quantitative Evidence for Bridged Structures in Asphaltenes by Thin Film Pyrolysis. *Energy Fuels* **2011**, *25*, 3581–3589, doi:10.1021/ef200518g.

33. Rüger, C.P.; Neumann, A.; Sklorz, M.; Schwemer, T.; Zimmermann, R. Thermal Analysis Coupled to Ultrahigh Resolution Mass Spectrometry with Collision Induced Dissociation for Complex Petroleum Samples: Heavy Oil Composition and Asphaltene Precipitation Effects. *Energy Fuels* **2017**, *31*, 13144–13158, doi:10.1021/acs.energyfuels.7b01778.

34. Chacón-Patiño, M.L.; Blanco-Tirado, C.; Orrego-Ruiz, J.A.; Gómez-Escudero, A.; Combariza, M.Y. Tracing the Compositional Changes of Asphaltenes after Hydroconversion and Thermal Cracking Processes by High-Resolution Mass Spectrometry. *Energy Fuels* **2015**, *29*, 6330–6341, doi:10.1021/acs.energyfuels.5b01510.

35. Strausz, O.P.; Mojelsky, T.W.; Faraji, F.; Lown, E.M.; Peng, P.'a. Additional Structural Details on Athabasca Asphaltene and Their Ramifications. *Energy Fuels* 1999, *13*, 207–227, doi:10.1021/ef980274w.

36. Gray, M.R. Consistency of Asphaltene Chemical Structures with Pyrolysis and Coking Behavior. *Energy Fuels* 2003, *17*, 1566–1569, doi:10.1021/ef030015t.

37. Savage, P.E.; Klein, M.T.; Kukes, S.G. Asphaltene reaction pathways. 1. Thermolysis. *Ind. Eng. Chem. Proc. Des. Dev.* 1985, *24*, 1169–1174, doi:10.1021/i200031a046.

38. Savage, P.E.; Klein, M.T.; Kukes, S.G. Asphaltene reaction pathways. 3. Effect of reaction environment. *Energy Fuels* 1988, *2*, 619–628, doi:10.1021/ef00011a003.

39. Strausz, O.P.; Mojelsky, T.W.; Lown, E.M. The molecular structure of asphaltene: an unfolding story. *Fuel* 1992, *71*, 1355–1363, doi:10.1016/0016-2361(92)90206-4.

40. Strausz, O.P.; Mojelsky, T.W.; Lown, E.M.; Kowalewski, I.; Behar, F. Structural Features of Boscan and Duri Asphaltenes. *Energy Fuels* 1999, *13*, 228–247, doi:10.1021/ef980245l.

41. Marshall, A.G.; Rodgers, R.P. Petroleomics: chemistry of the underworld. *PNAS* 2008, *105*, 18090–18095, doi:10.1073/pnas.0805069105.

42. McKenna, A.M.; Marshall, A.G.; Rodgers, R.P. Heavy Petroleum Composition. 4. Asphaltene Compositional Space. *Energy Fuels* 2013, *27*, 1257–1267, doi:10.1021/ef301747d.

43. Podgorski, D.C.; Corilo, Y.E.; Nyadong, L.; Lobodin, V.V.; Bythell, B.J.; Robbins, W.K.; McKenna, A.M.; Marshall, A.G.; Rodgers, R.P. Heavy Petroleum Composition. 5. Compositional and Structural Continuum of Petroleum Revealed. *Energy Fuels* 2013, *27*, 1268–1276, doi:10.1021/ef301737f.

44. Rüger, C.P.; Grimmer, C.; Sklorz, M.; Neumann, A.; Streibel, T.; Zimmermann, R. Combination of Different Thermal Analysis Methods Coupled to Mass Spectrometry for the Analysis of Asphaltenes and Their Parent Crude Oils: Comprehensive Characterization of the Molecular Pyrolysis Pattern. *Energy Fuels* 2018, *32*, 2699–2711, doi:10.1021/acs.energyfuels.7b02762.

45. Giraldo-Dávila, D.; Chacón-Patiño, M.L.; McKenna, A.M.; Blanco-Tirado, C.; Combariza, M.Y. Correlations between Molecular Composition and Adsorption, Aggregation, and Emulsifying Behaviors

of PetroPhase 2017 Asphaltenes and Their Thin-Layer Chromatography Fractions. *Energy Fuels* 2018, *32*, 2769–2780, doi:10.1021/acs.energyfuels.7b02859.

46. Chacón-Patiño, M.L.; Rowland, S.M.; Rodgers, R.P. Advances in Asphaltene Petroleomics. Part 1: Asphaltenes Are Composed of Abundant Island and Archipelago Structural Motifs. *Energy Fuels* 2017, *31*, 13509–13518, doi:10.1021/acs.energyfuels.7b02873.

47. Putman, J.C.; Moulian, R.; Smith, D.F.; Weisbrod, C.R.; Chacón-Patiño, M.L.; Corilo, Y.E.; Blakney, G.T.; Rumancik, L.E.; Barrère-Mangote, C.; Rodgers, R.P.; et al. Probing Aggregation Tendencies in Asphaltenes by Gel Permeation Chromatography. Part 2: Online Detection by Fourier Transform Ion Cyclotron Resonance Mass Spectrometry and Inductively Coupled Plasma Mass Spectrometry. *Energy Fuels* 2020, doi:10.1021/acs.energyfuels.0c02158.

48. Chacón-Patiño, M.L.; Rowland, S.M.; Rodgers, R.P. Advances in Asphaltene Petroleomics. Part 2: Selective Separation Method That Reveals Fractions Enriched in Island and Archipelago Structural Motifs by Mass Spectrometry. *Energy Fuels* 2018, *32*, 314–328, doi:10.1021/acs.energyfuels.7b03281.

49. Rodgers, R.P.; Mapolelo, M.M.; Robbins, W.K.; Chacón-Patiño, M.L.; Putman, J.C.; Niles, S.F.; Rowland, S.M.; Marshall, A.G. Combating selective ionization in the high resolution mass spectral characterization of complex mixtures. *Faraday Discuss.* 2019, *218*, 29–51, doi:10.1039/c9fd00005d.

50. Chacón-Patiño, M.L.; Rowland, S.M.; Rodgers, R.P. Advances in Asphaltene Petroleomics. Part 3. Dominance of Island or Archipelago Structural Motif Is Sample Dependent. *Energy Fuels* 2018, *32*, 9106–9120, doi:10.1021/acs.energyfuels.8b01765.

51. Neumann, A.; Käfer, U.; Gröger, T.; Wilharm, T.; Zimmermann, R.; Rüger, C.P. Investigation of Aging Processes in Bitumen at the Molecular Level with High-Resolution Fourier-Transform Ion Cyclotron Mass Spectrometry and Two-Dimensional Gas Chromatography Mass Spectrometry. Energy & Fuels. *Energy Fuels* 2020, *34*, 10641–10654, doi:10.1021/ACS.ENERGYFUELS.0C01242.

52. Chacón-Patiño, M.L.; Vesga-Martínez, S.J.; Blanco-Tirado, C.; Orrego-Ruiz, J.A.; Gómez-Escudero, A.; Combariza, M.Y. Exploring Occluded Compounds and Their Interactions with Asphaltene Networks Using High-Resolution Mass Spectrometry. *Energy Fuels* 2016, *30*, 4550–4561, doi:10.1021/acs.energyfuels.6b00278.

53. Rüger, C.P.; Miersch, T.; Schwemer, T.; Sklorz, M.; Zimmermann, R. Hyphenation of Thermal Analysis to Ultrahigh-Resolution Mass Spectrometry (Fourier Transform Ion Cyclotron Resonance Mass Spectrometry) Using Atmospheric Pressure Chemical Ionization For Studying Composition and Thermal Degradation of Complex Materials. *Analytical Chemistry* 2015, *87*, 6493–6499, doi:10.1021/acs.analchem.5b00785.

54. Peng, P.'a.; Morales-Izquierdo, A.; Hogg, A.; Strausz, O.P. Molecular Structure of Athabasca Asphaltene: Sulfide, Ether, and Ester Linkages. *Energy Fuels* 1997, *11*, 1171–1187, doi:10.1021/ef970027c.

55. Douda, J.; Llanos, M.E.; Alvarez, R.; Franco, C.L.; La Fuente, J.A.M. de. Pyrolysis applied to the study of a Maya asphaltene. *Journal of Analytical and Applied Pyrolysis* 2004, *71*, 601–612, doi:10.1016/j.jaap.2003.08.011.

56. Qian, K.; Robbins, W.K.; Hughey, C.A.; Cooper, H.J.; Rodgers, R.P.; Marshall, A.G. Resolution and Identification of Elemental Compositions for More than 3000 Crude Acids in Heavy Petroleum by Negative-Ion Microelectrospray High-Field Fourier Transform Ion Cyclotron Resonance Mass Spectrometry. *Energy & Fuels* 2001, *15*, 1505–1511, doi:10.1021/ef010111z.

57. Strausz, O.P.; Torres, M.; Lown, E.M.; Safarik, I.; Murgich, J. Equipartitioning of Precipitant Solubles between the Solution Phase and Precipitated Asphaltene in the Precipitation of Asphaltene. *Energy Fuels* 2006, *20*, 2013–2021, doi:10.1021/ef060013j.

58. Zhao, Y.; Gray, M.R.; Chung, K.H. Molar Kinetics and Selectivity in Cracking of Athabasca Asphaltenes. *Energy Fuels* 2001, *15*, 751–755, doi:10.1021/ef000286t.

59. Hauser, A.; AlHumaidan, F.; Al-Rabiah, H.; Halabi, M.A. Study on Thermal Cracking of Kuwaiti Heavy Oil (Vacuum Residue) and Its SARA Fractions by NMR Spectroscopy. *Energy Fuels* 2014, *28*, 4321–4332, doi:10.1021/ef401476j.

60. Chiaberge, S.; Guglielmetti, G.; Montanari, L.; Salvalaggio, M.; Santolini, L.; Spera, S.; Cesti, P. Investigation of Asphaltene Chemical Structural Modification Induced by Thermal Treatments. *Energy Fuels* 2009, *23*, 4486–4495, doi:10.1021/ef900206n.

61. Douda, J.; Alvarez, R.; Navarrete Bolaños, J. Characterization of Maya Asphaltene and Maltene by Means of Pyrolysis Application. *Energy Fuels* 2008, *22*, 2619–2628, doi:10.1021/ef800024p.

62. Cho, Y.; Kim, Y.H.; Kim, S. Planar limit-assisted structural interpretation of saturates/aromatics/resins/asphaltenes fractionated crude oil compounds observed by Fourier transform ion cyclotron resonance mass spectrometry. *Anal. Chem.* 2011, *83*, 6068–6073, doi:10.1021/ac2011685.

63. Hsu, C.S.; Lobodin, V.V.; Rodgers, R.P.; McKenna, A.M.; Marshall, A.G. Compositional Boundaries for Fossil Hydrocarbons. *Energy Fuels* 2011, *25*, 2174–2178, doi:10.1021/ef2004392.

64. Lobodin, V.V.; Marshall, A.G.; Hsu, C.S. Compositional space boundaries for organic compounds. *Anal. Chem.* 2012, *84*, 3410–3416, doi:10.1021/ac300244f.

65. Gray, M.R.; Tykwinski, R.R.; Stryker, J.M.; Tan, X. Supramolecular Assembly Model for Aggregation of Petroleum Asphaltenes. *Energy Fuels* 2011, *25*, 3125–3134, doi:10.1021/ef200654p.

66. Karacan, O.; Kok, M.V. Pyrolysis Analysis of Crude Oils and Their Fractions. *Energy Fuels* 1997, 385–391.

67. Friesen, W.I.; Michaelian, K.H.; Long, Y.; Dabros, T. Effect of Solvent-to-Bitumen Ratio on the Pyrolysis Properties of Precipitated Athabasca Asphaltenes. *Energy Fuels* 2005, *19*, 1109–1115, doi:10.1021/ef040073u.

68. Huang, J. Characterization of Thermally Degraded Asphaltene Fractions Using Gel Permeation Chromatography. *Petroleum Science and Technology* 2007, *25*, 1313–1320, doi:10.1080/10916460500423536.

69. Murgich, J.; Abanero, J.A.; Strausz, O.P. Molecular Recognition in Aggregates Formed by Asphaltene and Resin Molecules from the Athabasca Oil Sand. *Energy Fuels* 1999, *13*, 278–286, doi:10.1021/ef980228w.

70. Murugan, P.; Mahinpey, N.; Mani, T. Thermal cracking and combustion kinetics of asphaltenes derived from Fosterton oil. *Fuel Processing Technology* 2009, *90*, 1286–1291, doi:10.1016/j.fuproc.2009.06.008.

71. Juyal, P.; McKenna, A.M.; Fan, T.; Cao, T.; Rueda-Velásquez, R.I.; Fitzsimmons, J.E.; Yen, A.; Rodgers, R.P.; Wang, J.; Buckley, J.S.; et al. Joint Industrial Case Study for Asphaltene Deposition. *Energy Fuels* 2013, *27*, 1899–1908, doi:10.1021/ef301956x.

72. Nali, M.; Corana, F.; Montanari, L. Pyrolysis/gas chromatography/mass spectrometry in the analysis of asphaltenes. *Rapid. Commun. Mass Spectrom.* 1993, *7*, 684–687, doi:10.1002/rcm.1290070728.

73. Rakotondradany, F.; Fenniri, H.; Rahimi, P.; Gawrys, K.L.; Kilpatrick, P.K.; Gray, M.R. Hexabenzocoronene Model Compounds for Asphaltene Fractions: Synthesis & Characterization. *Energy Fuels* 2006, *20*, 2439–2447, doi:10.1021/ef060130e.

74. Liao, Z.; Zhou, H.; Graciaa, A.; Chrostowska, A.; Creux, P.; Geng, A. Adsorption/Occlusion Characteristics of Asphaltenes: Some Implication for Asphaltene Structural Features. *Energy Fuels* 2005, *19*, 180–186, doi:10.1021/ef049868r.

75. Boduszynski, M.M.; McKay, J.F.; Latham, D.R. Asphaltenes, where are you? *Asphalt Paving Technology* 1980, *49*, 123–143.

76. McKenna, A.M.; Purcell, J.M.; Rodgers, R.P.; Marshall, A.G. Heavy Petroleum Composition. 1. Exhaustive Compositional Analysis of Athabasca Bitumen HVGO Distillates by Fourier Transform Ion Cyclotron Resonance Mass Spectrometry: A Definitive Test of the Boduszynski Model. *Energy Fuels* 2010, *24*, 2929–2938, doi:10.1021/ef100149n.

77. *The Boduszynski continuum*. *Contributions to the understanding of the molecular composition of petroleum;* Ovalles, C.; Moir, M.E., Eds.; American Chemical Society; Distributed in print by Oxford University Press: Washington, DC, 2018, ISBN 0-8412-3294-6.

78. Ruiz-Morales, Y. HOMO−LUMO Gap as an Index of Molecular Size and Structure for Polycyclic Aromatic Hydrocarbons (PAHs) and Asphaltenes: A Theoretical Study. I. *J. Phys. Chem. A* 2002, *106*, 11283–11308, doi:10.1021/jp021152e.

79. Frakman, Z.; Ignasiak, T.M.; Lown, E.M.; Strausz, O.P. Oxygen compounds in Athabasca asphaltene. *Energy Fuels* 1990, *4*, 263–270, doi:10.1021/ef00021a008.

80. Cheshkova, T.V.; Sergun, V.P.; Kovalenko, E.Y.; Gerasimova, N.N.; Sagachenko, T.A.; Min, R.S. Resins and Asphaltenes of Light and Heavy Oils: Their Composition and Structure. *Energy Fuels* 2019, *33*, 7971–7982, doi:10.1021/acs.energyfuels.9b00285.

81. Giraldo-Dávila, D.; Chacón-Patiño, M.L.; Orrego-Ruiz, J.A.; Blanco-Tirado, C.; Combariza, M.Y. Improving compositional space accessibility in (+) APPI FT-ICR mass spectrometric analysis of crude oils by extrography and column chromatography fractionation. *Fuel* 2016, *185*, 45–58, doi:10.1016/j.fuel.2016.07.096.

82. Cho, Y.; Na, J.-G.; Nho, N.-S.; Kim, S.; Kim, S. Application of Saturates, Aromatics, Resins, and Asphaltenes Crude Oil Fractionation for Detailed Chemical Characterization of Heavy Crude Oils by Fourier Transform Ion Cyclotron Resonance Mass Spectrometry Equipped with Atmospheric Pressure Photoionization. *Energy Fuels* 2012, *26*, 2558–2565, doi:10.1021/ef201312m.

83. Clingenpeel, A.C.; Rowland, S.M.; Corilo, Y.E.; Zito, P.; Rodgers, R.P. Fractionation of Interfacial Material Reveals a Continuum of Acidic Species That Contribute to Stable Emulsion Formation. *Energy Fuels* 2017, *31*, 5933–5939, doi:10.1021/acs.energyfuels.7b00490.

84. Gaspar, A.; Zellermann, E.; Lababidi, S.; Reece, J.; Schrader, W. Characterization of Saturates, Aromatics, Resins, and Asphaltenes Heavy Crude Oil Fractions by Atmospheric Pressure Laser Ionization Fourier Transform Ion Cyclotron Resonance Mass Spectrometry. Energy & Fuels, 26(6), 3481-3487 2012, doi:10.1021/EF3001407.

85. Buenrostro-Gonzalez, E.; Andersen, S.I.; Garcia-Martinez, J.A.; Lira-Galeana, C. Solubility/Molecular Structure Relationships of Asphaltenes in Polar and Nonpolar Media. *Energy Fuels* 2002, *16*, 732–741, doi:10.1021/ef0102317.

86. Buenrostro-Gonzalez, E.; Groenzin, H.; Lira-Galeana, C.; Mullins, O.C. The Overriding Chemical Principles that Define Asphaltenes. *Energy Fuels* 2001, *15*, 972–978, doi:10.1021/ef0100449.

87. Moldoveanu, S.C. Chapter 7 Pyrolysis of Hydrocarbons. In *Pyrolysis of organic molecules with applications to health and environmental issues,* 1st ed.; Moldoveanu, Ș., Ed.; Elsevier: Amsterdam, London, 2010; pp 131–229, ISBN 9780444531131.

88. Corilo, Y.E.; Rowland, S.M.; Rodgers, R.P. Calculation of the Total Sulfur Content in Crude Oils by Positive-Ion Atmospheric Pressure Photoionization Fourier Transform Ion Cyclotron Resonance Mass Spectrometry. *Energy Fuels* 2016, *30*, 3962–3966, doi:10.1021/acs.energyfuels.6b00497.

89. Lobodin, V.V.; Robbins, W.K.; Lu, J.; Rodgers, R.P. Separation and Characterization of Reactive and Non-Reactive Sulfur in Petroleum and Its Fractions. *Energy Fuels* 2015, *29*, 6177–6186, doi:10.1021/acs.energyfuels.5b00780.

90. Brodbelt, J.S. Photodissociation mass spectrometry: new tools for characterization of biological molecules. *Chem. Soc. Rev.* 2014, *43*, 2757–2783, doi:10.1039/c3cs60444f.

Supplemental Material

Investigation of island/ single core and archipelago/ multicore enriched asphaltenes and their solubility fractions by thermal analysis coupled to high resolution Fourier transform ion cyclotron resonance mass spectrometry

Anika Neumann[1,2], Martha Liliana Chacón-Patiño[3], Ryan P. Rodgers[3], Christopher P. Rüger[1,2]*, Ralf Zimmermann[1,2,4]

1 –Joint Mass Spectrometry Centre (JMSC)/Chair of Analytical Chemistry, University of Rostock, 18059 Rostock, Germany

2 – Department Life, Light & Matter (LLM), University of Rostock, 18051 Rostock, Germany

3 – National High Magnetic Field Laboratory and Florida State University, Tallahassee, Florida 32310, United States

4 – Joint Mass Spectrometry Centre (JMSC)/Helmholtz Zentrum München, Comprehensive Molecular Analytics, 85764 Neuherberg, Germany

Keywords: asphaltenes, thermal analysis, high-resolution mass spectrometry, pyrolysis, extrography

* corresponding author, christopher.rueger@uni-rostock.de

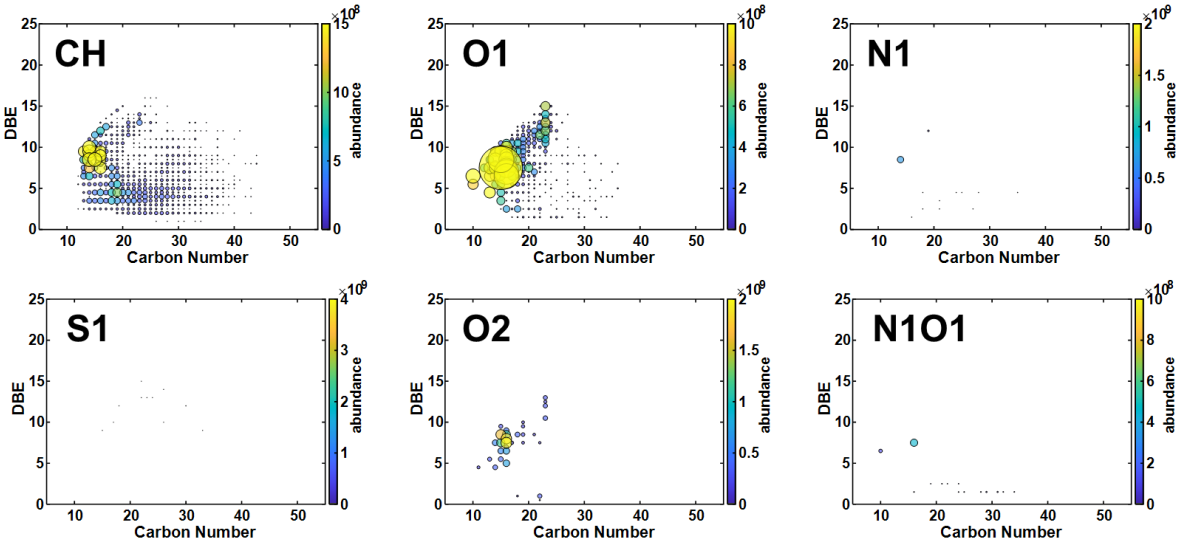

Figure S 1: DBE vs. #C-diagrams of the main compound classes of occluded compounds of the Hep/Tol fraction of Wyoming asphaltenes.

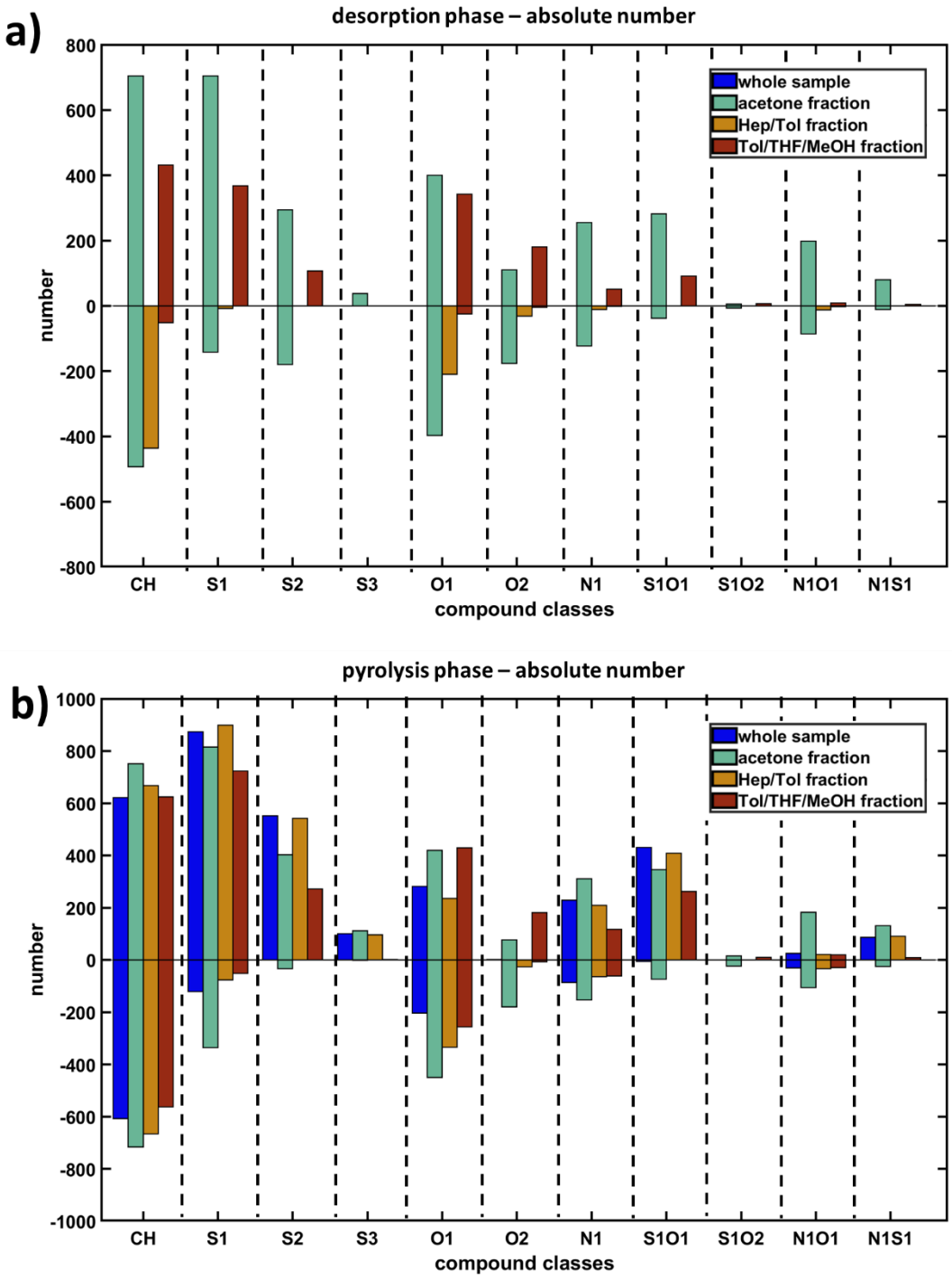

Figure S 2: Overview on the number of the assigned sum formulae of the compound classes of the whole asphaltenes and their fraction for a) the desorption phase and b) the pyrolysis phase.

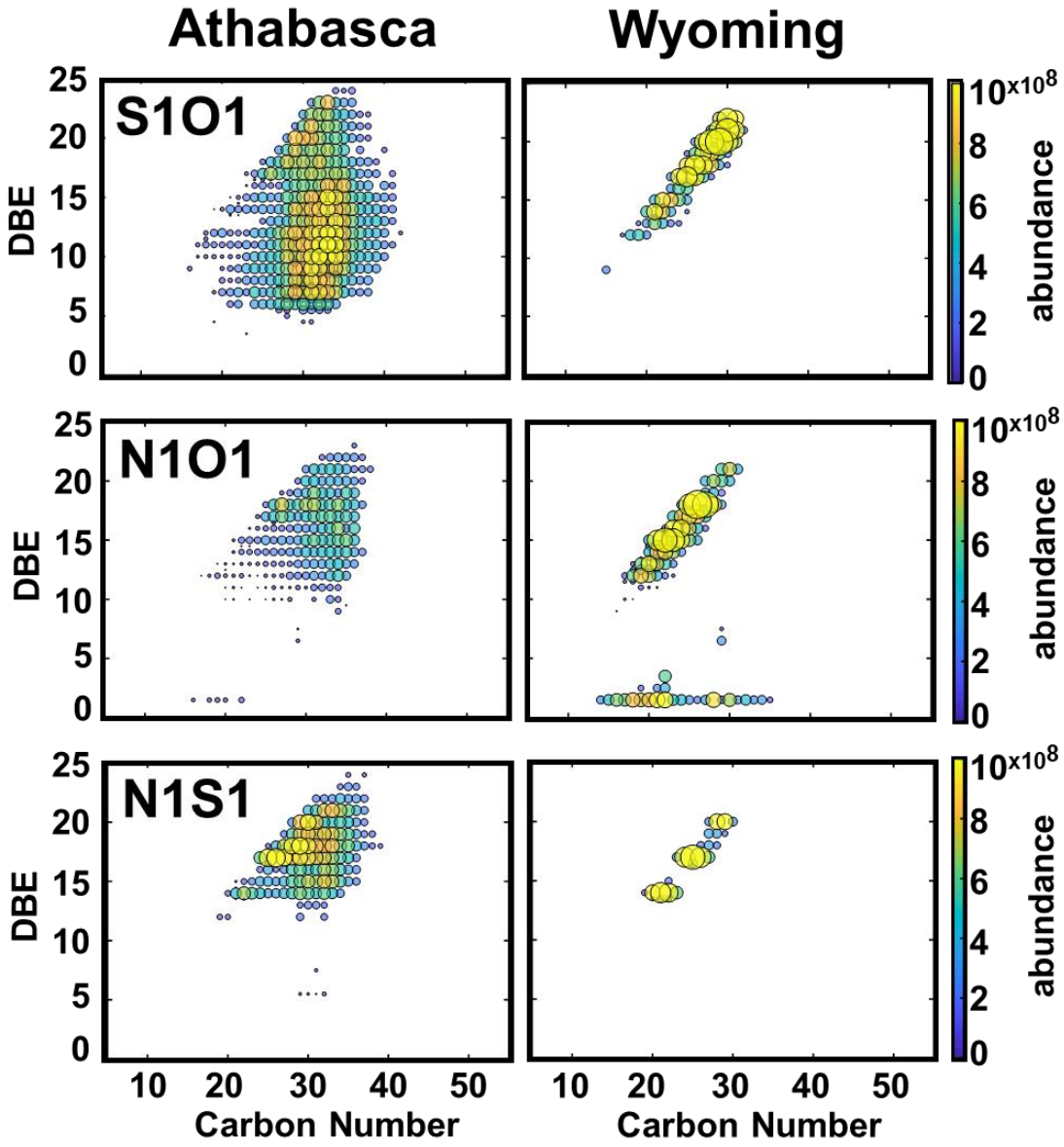

Figure S 3: DBE vs. #C-diagrams of the pyrolysis fragments of asphaltenes eluted with acetone for the S1O1-, N1O1- and N1S1-class.